NASA
Technical
Paper
2370

November 1984

Fracture Toughness of Fibrous Composite Materials

C. C. Poe, Jr.

NASA

DISCLAIMER NOTICE

THIS DOCUMENT IS BEST QUALITY AVAILABLE. THE COPY FURNISHED TO DTIC CONTAINED A SIGNIFICANT NUMBER OF PAGES WHICH DO NOT REPRODUCE LEGIBLY.

NASA Technical Paper 2370

1984

Fracture Toughness of Fibrous Composite Materials

C. C. Poe, Jr.

Langley Research Center
Hampton, Virginia

NASA
National Aeronautics
and Space Administration

Scientific and Technical Information Branch

CONTENTS

INTRODUCTION

Fibrous composite materials are as strong as steel, have a lower density than magnesium, and can be tailored to have maximum strength and stiffness in specific directions. Thus, composite structures are potentially much lighter than conventional metallic structures, but they are also very notch sensitive because of the linear-elastic fibers that carry most of the load.

Figure 1 illustrates the notch sensitivity of composites compared with metals, as well as the extensive range of composite properties. Fracture toughness K_Q is plotted against ultimate tensile strength F_{tu} for Thornel 300 (T300)[1] graphite/epoxy laminates and metals. All aluminums, steels, and titanium fall within the "metals" region, and all $[0_m/\pm45_n/90_p]_s$ and $[0_m/\pm\alpha_n]_s$ laminate orientations or lay-ups fall within the "composites" region. (The 0° direction corresponds to the loading direction.) The K_Q and F_{tu} values were divided by density to show the relative efficiencies of the composites and metals.

The ratio of K_Q to F_{tu} is, in first approximation, proportional to strength retention (the ratio of cracked strength to F_{tu}) for a given crack length. More strength retention means less notch sensitivity. For the composites, the strength retention for a 5-mm through-the-thickness crack ranges from 51 to 90 percent, depending on lay-up. The strength retention is greater than 90 percent for many metals, but it would, of course, be less for longer cracks and vice versa. Thus, for many lay-ups, the composites are more notch sensitive than metals.

The fracture toughness of composites depends on fiber and matrix properties as well as lay-up. There are literally infinite combinations of fiber, matrix, and lay-up - far too many to evaluate experimentally. Thus, some guidance and analysis are needed to select fiber, matrix, and lay-up to give maximum fracture toughness for a given strength and stiffness.

The general fracture-toughness parameter developed in references 1 and 2 provides such an analysis. With it, the fracture toughness can be predicted for any fibrous composite lay-up in terms of the elastic constants and the fiber failing strain. The boundaries of the composites region in figure 1 were predicted with this analysis. The present paper reports the results of an investigation to evaluate the accuracy of this analysis and determine its limitations.

For this purpose, numerous laminates with various proportions of 0°, ±45°, and 90° plies were fabricated from T300/5208[2] and T300/BP-907[3] graphite/epoxy prepreg tape material. The strength of the BP-907 resin is about 1.5 times that of the 5208 resin. Specimens were cut from the laminates, and cracklike slots were machined in the center of the specimens. Maximum failing loads were measured, and values of

---

[1]Thornel 300 (T300): Registered trademark of Union Carbide Corporation.
[2]5208: Registered trademark of Narmco Materials Corporation.
[3]BP-907: Registered trademark of American Cyanamid Company.

fracture toughness were computed and compared with predicted values. Radiographs were made of some specimens to determine the extent of matrix splitting at the crack tips. Crack-tip splitting was also predicted by using the local stress field and compared with the splitting revealed by the radiographs.

Also, a parametric study was made to determine how fiber and matrix properties as well as lay-up influence the predicted values of fracture toughness. Both $[0_m/\pm45_n/90_p]_s$ and $[0_m/\pm\alpha_n]_s$ lay-ups were considered.

SYMBOLS

a	half-length of crack or slot, m
B_0, B_1, B_2	coefficients of a series
C_1, C_2	functions
$\{D\}$	column matrix of functions
d_o	characteristic distance, m
E	Young's modulus, Pa
F	uncracked strength, Pa
G	shear modulus, Pa
H_1, H_2	functions
K	stress-intensity factor, $Pa\text{-}m^{1/2}$
K_Q	critical stress-intensity factor (fracture toughness), $Pa\text{-}m^{1/2}$
K_{Qe}	elastic critical stress-intensity factor, $Pa\text{-}m^{1/2}$
$K_{Q\varepsilon}$	critical strain-intensity factor, $m^{1/2}$
ℓ_α	split length in direction α, m
$\ell_{1\alpha}, \ell_{2\alpha}, \ell_{12\alpha}$	components of ℓ_α, m
M_1, M_2, M_{12}	elements of column matrix
m,n,p	matrix or number of plies
N	factor indicating how many times plies are repeated in a lay-up
N_o	number of ply orientations in quasi-isotropic lay-ups
$[Q]$	matrix of lamina constants, Pa
Q_c	general fracture-toughness parameter, $m^{1/2}$
r, θ	polar coordinates

S	applied gross laminate stress, Pa
$[T]$	tensor transformation matrix
V_f	fiber volume fraction
W	specimen width, m
x,y	Cartesian variables (see fig. 3)
α	fiber orientation angle relative to loading axis, deg
α^*	angle of principal load-carrying plies, deg
$[\beta]$	matrix of laminate constants, Pa^{-1}
γ	shear strain
ε	axial strain
ε_o	far-field strain in y-direction
λ	proportion of 0° plies, $\lambda = m/(m + 2n + p)$
μ_1, μ_2	complex roots of characteristic equation
ν	Poisson's ratio
ξ	function
ρ	density, $kg\text{-}m^{-3}$
σ	axial stress, Pa
τ	shear stress, Pa

Subscripts:

c	failure
m	matrix or number of 0° plies
N	factor indicating how many times plies are repeated in a lay-up
n	number of ±45° plies or ±α plies
net	stress based on net area
p	number of 90° plies
s	symmetric condition
tu	tensile ultimate
tuf	tensile ultimate of fiber

u	ultimate
x,y	Cartesian coordinates (where x refers to the 90° fiber direction)
α	plies with angle α
1,2	principal ply coordinates (where 1 refers to the fiber direction and 2 refers to the normal to the fiber direction)

Abbreviation:

COV	coefficient of variation

The following notation is used to prescribe the laminate orientation or lay-up. Ply angles are separated by a slash and are listed in the order of lay-up. A numerical subscript on the ply angle denotes how many consecutive plies are at that angle. The subscript s, which is outside the brackets that enclose the listing, denotes a symmetric condition. A numerical factor of s denotes how many times the plies within the brackets are repeated. (The $\bar{0}$ indicates that the 0° ply is not repeated but lies in the plane of symmetry.) For example, $[0_2/\pm45]_{2s}$ means [0/0/45/-45/0/0/45/-45/-45/45/0/0/-45/45/0/0]. The subscript T outside the brackets denotes total; for example, $[0]_{6T}$ means [0/0/0/0/0/0].

EXPERIMENTS

Materials and Specimens

Graphite/epoxy laminates were made from prepreg tape material with T300 fiber and both 5208 and BP-907 resins. Since the 5208 prepreg material was bought several years before the BP-907 material, the T300 fibers for the two materials were probably not from the same batch.

The stress-strain curves for the 5208 and BP-907 neat resins from reference 3 are plotted in figure 2. The strength of the BP-907 resin is about 1.5 times that of the 5208 resin. The initial moduli are about the same.

The 5208 laminates were made by the Douglas Aircraft Company, and the BP-907 laminates were made by the Fabrication Division at the Langley Research Center. The laminates were made with various proportions of 0°, ±45°, and 90° plies. Eleven different lay-ups (combinations of ply orientations) were made with the 5208 prepreg material and four were made with the BP-907 material. (See table I.) The same combinations of ply orientations were used for the 5208 and BP-907 laminates except for the quasi-isotropic lay-ups, in which the number of plies in the BP-907 laminate was twice that in the 5208 laminate.

The laminates were cured at 450 K (350°F) according to the suppliers' recommended cure cycle and were ultrasonically examined by using a C-scan. The C-scans for the $[45/0/-45/0]_{2s}$ and $[45/0/-45/90]_{2s}$ BP-907 laminates were attenuated more than for the other laminates. The large attenuation could have been caused, at least partially, by rough surfaces that appeared to be wrinkled by the vacuum bag during cure. Caul plates were used to cure all but these two laminates. Despite the high attenuation, the mechanical behavior of these two laminates seemed normal.

The laminates were cut into rectangular specimens by means of diamond cutters. The specimen configuration is shown in figure 3. The free length between grips was at least twice the width. Cracklike slots were ultrasonically cut completely through the specimens at their centers. The 0.4-mm-wide slots were oriented normal to the loading axis and were never longer than half the specimen width. The slot lengths 2a and specimen widths W are given in the following table:

Slot lengths, 2a, mm, for W of -		
50 mm	100 mm	305 mm
BP-907		
5.0 10.0 20.0	20.0 40.0	
5208		
	10.3 20.3 30.5 50.8	30.5 61.0 91.4 152.4

Note that the y-axis in figure 3 is normal to the crack and parallel to the 0° fiber direction. Although this convention is consistent with fracture-mechanics literature, it unfortunately is inconsistent with composite-materials literature. The x and y subscripts on the elastic constants herein are reversed to those in most composite-materials literature.

Fiber volume fractions are reported in table I. They were determined by drying small coupons, measuring their mass, digesting the matrix, and measuring their remaining mass. Fiber volume fractions for the 5208 laminates were about 15 percent larger than those for the BP-907 laminates.

The specimens were stored several years at ambient conditions before they were tested. The moisture mass fraction ranged between 0.6 and 0.9 percent at the time of testing and was determined by weighing coupons before and after drying. The coupons were cut from failed specimens.

Some of the $[\pm 45/0/\pm 45/\bar{0}]_s$ T300/5208 laminates were incorrectly made to be $[\pm 45/0/\mp 45/0/\pm 45/0/\pm 45]_T$, which is unsymmetric. However, no differences between the mechanical responses of the symmetric and unsymmetric laminates were discernible. Also, one of the $[45/0/-45/90]_s$ 5208 laminates and one of the $[45/0/-45/90]_{2s}$ BP-907 laminates were rotated 90° so that the 0° and 90° plies were interchanged. The only noticeable difference in behavior between laminates with the two stacking sequences was in the ultimate tensile strengths of the 5208 laminates. The laminate with 90° plies in the middle delaminated at a high stress because of large interlamina tensile stresses at the free edge, whereas the laminate with 0° plies in the middle did not. The specimens with the stronger BP-907 resin did not appear to delaminate in either case.

Values of the elastic constants for each lay-up and material are reported in table I. The elastic constants were calculated with lamination theory by using the $[0]_{8T}$ constants in table I as lamina constants. For the $[0]_{8T}$ laminate, the Young's moduli and Poisson's ratios were determined from tensile stress-strain data. The shear modulus was determined from tensile stress-strain data for $[\pm 45]_{2s}$ laminates. Reference 4 contains tensile stress-strain data for all of these 5208 laminates. Differences between calculated and measured elastic constants were within experimental inaccuracies.

Stresses were calculated from loads by using average ply thicknesses of 0.140 mm and 0.156 mm for the T300/5208 and T300/BP-907 laminates, respectively. The larger ply thickness and lower moduli and strengths of the T300/BP-907 laminates reflect their lower fiber volume fraction. (See table I.)

Procedure

The fracture tests were conducted under ambient conditions in displacement-controlled testing machines of either 89 or 534 kN capacity. The specimens were loaded to failure with crosshead speeds of 0.5 and 1.3 mm/min. The lowest speed was used for the stiffest laminates with the result that loading rates were uniformly small. Strain readings were continuously recorded against load on x-y recorders.

Thin center-cracked specimens tend to buckle above and below the slots because of compressive stresses σ_x, which are equal in magnitude to the applied stress. Strengths are usually lower when the buckles develop. Because fracture-mechanics analyses cannot readily account for these buckles, the buckles were prevented by sandwiching the specimen between two relatively thick aluminum plates. To eliminate friction, Teflon[4] sheets were placed between the specimen and the plates, and the bolts that provided the clamping force were only finger tightened.

A few of the 50-mm-wide specimens were radiographed with an industrial-type "soft" X-ray machine. A tetrabromoethane or zinc iodide solution, which is more opaque to X-rays than graphite/epoxy, was injected at the slit ends to outline matrix damage. Fracture results for the 50-mm-wide 5208 specimens are not presented because only a few 50-mm-wide specimens were tested.

Strain gages were located on both sides near one end of each specimen to measure far-field strain. Except for the $[0]_{8T}$, $[0_2/90/0]_s$, $[0_2/45/0_2/-45/0_2]_s$, $[90/0]_{2s}$, and $[\pm 45]_{2s}$ specimens, the strain-gauge readings were usually within ±5 percent of the value for uniaxial stress. For the $[0]_{8T}$, $[0_2/90/0]_s$, $[0_2/45/0_2/-45/0_2]_s$, and $[90/0]_{2s}$ specimens, readings were below the uniaxial values because long 0° splits developed at the slot ends.

For the $[\pm 45]_{2s}$ specimens, the strain-gauge readings were as much as 1.5 times the uniaxial values. These readings were elevated by the rigid grips, which prevented the large transverse contractions associated with this particular lay-up. A finite-element analysis indicated that although the strain-gauge readings were elevated by the grips, the stress-intensity factor was virtually identical to that for an infinitely long specimen subjected to uniaxial stress.

---

[4]Teflon: Registered trademark of E. I. du Pont de Nemours & Company, Inc.

Except for the $[0]_{8T}$ specimens, the gross failing stress and the ratio S_{net}/F_{tu} are given in tables II and III for the 5208 and BP-907 specimens, respectively. The values for the $[0]_{8T}$ specimens are not reported because the specimens split to the grips and failed with $S_{net} = F_{tu}$.

ANALYSIS

Fracture-Toughness Calculations

Critical values of the stress-intensity factor or fracture toughness K_Q were calculated with

$$K_Q = K_{Qe}\left(1 - \frac{K_{Qe}^2}{\pi a F_{tu}^2}\right)^{-1/2} \tag{1}$$

where

$$K_{Qe} = S_c[\pi a \sec(\pi a/W)]^{1/2}$$

is the usual elastic stress-intensity factor (refs. (1) and (2)), S_c is the gross failing stress, a is the slot half-length, and $[\sec(\pi a/W)]^{1/2}$ is an isotropic, finite-width correction factor. The isotropic correction factor is reasonably accurate for the specially orthotropic laminates. For long cracks, $K_{Qe}^2/\pi a F_{tu}^2 \ll 1$ and $K_Q \approx K_{Qe}$; and for $a = 0$, equation (1) gives $S_c = F_{tu}$. Values of K_Q calculated with equation (1) are given in tables II and III for each specimen. Average values of K_Q and coefficients of variation (COV) are reported in table IV for each lay-up. The measured F_{tu} values in table I for lay-ups with 0° plies were not used in equation (1). They are suspect because the failing strains vary from 0.00769 to 0.0116. Therefore, F_{tu} values calculated by $E_y\varepsilon_{tuf}$, where $\varepsilon_{tuf} = 0.010$, were used in lieu of the measured values. They are shown within parentheses in table I. For lay-ups without 0° plies, the actual measured values of F_{tu} in table I were used in equation (1).

Fracture-Toughness Predictions

In references 1 and 2, a general fracture-toughness parameter that can be used to predict the fracture toughness of composite laminates was derived. The predictions require only the elastic constants of the laminate and the ultimate tensile failing strain of the fibers ε_{tuf}. The derivation is briefly repeated for convenience as follows:

First, attention was directed to the principal load-carrying plies. These plies are the stiffest and strongest plies in a laminate with respect to the loading direction, and they carry most of the load. Consequently, their failure is sufficient to cause the failure of all other plies. Thus for the lay-ups in table I, the principal load-carrying plies are the 0° plies, except for the $[90/45/90/-45]_s$ and $[\pm 45]_{2s}$ lay-ups in which they are the 45° plies.

Next, failure of the principal load-carrying plies was predicted by using a maximum-strain criterion. At failure, the fiber strains ahead of a crack tip in a specially orthotropic laminate under plane stress and mode I conditions are given by

$$\varepsilon_{1c} = Q_c(2\pi r)^{-1/2} + B_0 + B_1 r^{1/2} + B_2 r^{3/2} + \ldots \tag{2}$$

where r is the distance from the crack tip. The coefficient Q_c is the general fracture-toughness parameter given by

$$Q_c = K_Q \xi / E_y \tag{3}$$

where K_Q is the critical value of the stress-intensity factor or fracture toughness and

$$\xi = \left[1 - \nu_{yx}(E_x/E_y)^{1/2}\right]\left[(E_y/E_x)^{1/2} \sin^2 \alpha^* + \cos^2 \alpha^*\right]$$

The constants E_x, E_y, and ν_{yx} are the usual extensional elastic constants of the laminate, and α^* is the angle that the principal load-carrying fibers make with the y-axis.

At failure, the critical level of fiber strains in the principal load-carrying plies just ahead of the crack tip was assumed to be the same, regardless of lay-up. Furthermore, the critical strain level was assumed to increase in proportion to the ultimate tensile failing strain of the fibers ε_{tuf}. This criterion is equivalent to a "point-strain" criterion applied to the principal load-carrying plies. That is, at failure, $\varepsilon_{1c} = \varepsilon_{tuf}$ at $r = d_o$ in equation (2). By retaining only the $r^{-1/2}$ term, equation (2) gives

$$\frac{Q_c}{\varepsilon_{tuf}} = (2\pi d_o)^{1/2}$$

which is a constant for all composite laminates, independent of lay-up and material.

In reference 2, values of Q_c/ε_{tuf} were calculated for numerous materials and lay-ups. A representative value of 1.5 $mm^{1/2}$ (where $d_o = 0.36$ mm) was obtained for laminates with small crack-tip damage, and it was much larger for laminates that developed long 0° splits at the crack tips. Equation (2) does not take splits into account and is not valid in this case. Replacing Q_c by $1.5\varepsilon_{tuf}$ $mm^{1/2}$ in equation (3) and solving for K_Q gives

$$K_Q = 1.5\varepsilon_{tuf} E_y / \xi \tag{4}$$

Values of K_Q were predicted with equation (4) for each lay-up by using the elastic constants in table I and $\varepsilon_{tuf} = 0.010$, and they are listed in table IV.

RESULTS

Crack-Tip Damage

$[0]_{8T}$, $[0_2/90/0]_s$, $[0_2/45/0_2/-45/0_2]_s$, and $[90/0]_{2s}$ specimens.- Splits developed at the slot ends in the 0° plies before overall failure, as seen by the radiographs in figure 4 that were made near failure. (These results are representative of other slot lengths and specimen widths.) The plane normal to the laminate that contains the split is relatively weak because 50 percent or more of the plies are 0° plies. For the $[0]_{8T}$ specimens, the splits initiated at relatively small loads and extended to the grips well before failure. Consequently, the stress-concentration factor was reduced to unity, and the ligaments failed with $S_{net} = F_{tu}$. The strain-gauge readings indicated that specimens with the 5208 matrix split at lower stresses than those with the stronger BP-907 matrix.

Of the $[0_2/90/0]_s$, $[0_2/45/0_2/-45/0_2]_s$, and $[90/0]_{2s}$ specimens, splits were longest in the $[0_2/90/0]_s$ specimens and shortest in the $[90/0]_{2s}$ specimens. Usually, the splits did not extend to the specimen ends. The radiographs in figure 4 also indicate that the 0° and off-axis plies delaminated in a narrow region along the splits of the $[0_2/90/0]_s$ and $[0_2/45/0_2/-45/0_2]_s$ specimens, but not in the $[90/0]_{2s}$ specimens. The delaminations reduced the effectiveness of the off-axis plies to retard splitting. Consequently, delaminations made the splits longer.

Fracture paths were self-similar (coincided with a line containing the slot) in the $[90/0]_{2s}$ specimens, but not always in the $[0_2/90/0]_s$ and $[0_2/45/0_2/-45/0_2]_s$ specimens. When the fractures were not self-similar, they initiated in the splits some distance above or below the ends of the slot, as seen in the photographs of failed specimens in figure 5.

The 0° splits in these specimens were long enough to affect the remote strain-gauge readings. As the splits lengthened, the readings fell below the strains associated with a uniaxial state of stress. For the $[0]_{8T}$ specimens, the readings virtually fell to zero because the splits extended past the gauges to the grips.

$[90/0/90/0/45/0/-45/0]_s$, $[45/0/-45/0]_s$, $[45/0/-45/0]_{2s}$, $[\pm45/0/\pm45/\bar{0}]_s$, and $[45/0/-45/90]_s$ 5208 specimens and $[45/0/-45/0]_{2s}$ and $[45/0/-45/90]_{2s}$ BP-907 specimens.- The radiographs in figure 4 do not reveal 0° splits. If any exist, they are relatively small. However, the radiographs do reveal splits in the ±45° and 90° plies of most specimens, and they also reveal delaminations within the sectors between ±45° splits in the $[\pm45/0/\pm45/\bar{0}]_s$ and $[45/0/-45/90]_s$ 5208 specimens. The ±45° splits were much smaller in the BP-907 specimens. Also, the radiographs of BP-907 specimens did not reveal 90° splits nor delaminations. Thus, crack-tip damage was much less in the stronger BP-907 matrix than in the 5208 matrix.

Fracture paths for this group of specimens were self-similar except for the $[\pm45/0/\pm45/\bar{0}]_s$ specimens, in which the fractures usually extended to the specimen edge at 45° to the slot. These specimens also delaminated along the fracture path. (See fig. 5.)

In general, the surface plies of the 5208 specimens tended to peel along the fracture path, whereas the surface plies of the BP-907 specimens cohered.

$[\pm 45]_{2s}$ and $[90/45/90/-45]_s$ specimens.- Splits can also be seen in figure 4 at the slot ends in the ±45° plies of these specimens. They were much smaller in the $[\pm 45]_{2s}$ BP-907 specimen than in the $[\pm 45]_{2s}$ 5208 specimen. In addition, splits can be seen in the 90° plies within the net section of the $[90/45/90/-45]_s$ specimen.

The fracture path in the $[\pm 45]_{2s}$ 5208 specimen in figure 5 was not self-similar. For the 100-mm-wide specimens, the path usually extended from each slot end to the specimen edge at a 45° angle, and the specimens delaminated along the fracture path. Thus, failure was via matrix and not fiber. For the 305-mm-wide specimens, the fracture path was initially self-similar; but after the fracture extended a short distance, the path turned and proceeded to the specimen edge along a 45° angle like the 100-mm-wide specimens. In contrast, the fracture path in the $[\pm 45]_{2s}$ BP-907 specimens was largely self-similar, with little delamination. Thus, failure was via fiber.

Splitting Predictions

Equation (13) in the appendix was used to predict the lengths of splits ℓ_α emanating from the crack tips. It was derived by using the Tsai-Hill failure criterion (ref. 5) and the singular stress field given by the theory of elasticity. Table V contains the values of ℓ_α for each ply orientation of each lay-up in table I.

In addition, $\ell_{1\alpha}$, $\ell_{2\alpha}$, and $\ell_{12\alpha}$, which are the contributions to ℓ_α from the lamina stresses σ_1, σ_2, and τ_{12}, respectively, are given in table V. They also correspond to split lengths predicted by the maximum-stress criterion. Thus, the relative values of $\ell_{1\alpha}$, $\ell_{2\alpha}$, and $\ell_{12\alpha}$ indicate which stress components are the principal cause of splitting in the various plies.

The values of ℓ_α in table V are largest for the 0° plies of the $[0]_{8T}$, $[0_2/90/0]_s$, $(0_2/45/0_2/-45/0_2]_s$, and $[90/0]_{2s}$ lay-ups, much like the radiographs indicated. The $\ell_{12\alpha}$ values are small except for the 0° plies of the aforementioned lay-ups and $[\pm 45]_{2s}$. (For the 90° plies, $\ell_{12\alpha} = 0$ because of symmetry.) The $\ell_{1\alpha}$ values are small for all the lay-ups but, on the other hand, the $\ell_{2\alpha}$ values are large for all the plies that tended to split. Thus, the σ_2 stress is probably the principal cause of the splitting observed in the radiographs of figure 4. The τ_{12} stress contributes only to the splitting of the 0° plies in the $[0]_{8T}$, $[0_2/90/0]_s$, $[0_2/45/0_2/-45/0_2]_s$, and $[90/0]_{2s}$ laminates and of the 45° plies in the $[\pm 45]_{2s}$ laminate.

The ℓ_α values in table V for the BP-907 laminates are less than half those for the corresponding 5208 laminates. Recall that the strength of the BP-907 epoxy is about 1.5 times that of the 5208, and split length decreases with the square of the allowable stresses.

The values of ℓ_α are also drawn to scale in figure 6 for each laminate. The predicted split patterns agree with those in the radiographs in figure 4. However, the lengths of 0° splits in the $[0]_{8T}$, $[0_2/90/0]_s$, and $[0_2/45/0_2/-45/0_2]_s$ 5208 specimens and of 45° splits in the $[90/45/90/-45]_s$ and $[\pm 45]_{2s}$ 5208 specimens were

greatly underestimated for the following reasons: (1) The predicted K_Q values in table IV were underestimated, as will be discussed later; and (2) the singular stress field in the appendix does not take the splits into account and, thus, the local stresses are underestimated, especially when ℓ_α is large.

Fracture Toughness and Strengths

The measured values of fracture toughness in table IV were divided by the predicted values and are plotted in figure 7. Three ratios are shown for each lay-up. The middle value represents the average measured value, and the other two values are one plus and one minus the coefficient of variation (COV). Thus, the difference between the highest and lowest values for each lay-up represents two standard deviations. The ±0.10 region about unity represents a typical coefficient of variation for F_{tu} of unidirectional graphite/epoxy specimens. The fracture specimens should have the same coefficient of variation if the failures are via fibers.

The measured strengths in tables II and III are plotted against slot length as symbols in figures 8 and 9. Predicted strengths are plotted as solid lines for comparison. They were calculated by use of equation (1) with the predicted K_Q values in table IV. In order for the predictions to be independent of specimen width, the strengths were multiplied by the finite-width correction factor $[\sec(\pi a/W)]^{1/2}$. Solving equation (1) gives

$$S_c[\sec(\pi a/W)]^{1/2} = K_Q\left(\pi a + \frac{K_Q^2}{F_{tu}^2}\right)^{1/2} \tag{5}$$

As before, values of $F_{tu} = E_y\varepsilon_{tuf}$ were used in equation (5) for lay-ups with 0° plies, and measured values in table I were used for lay-ups without 0° plies.

Since the net-section stress is limited to F_{tu}, strengths are limited to

$$S_c[\sec(\pi a/W)]^{1/2} = F_{tu}\left(1 - \frac{2a}{W}\right)[\sec(\pi a/W)]^{1/2}$$

which is plotted for the different specimen widths as dashed lines in figures 8 and 9.

For convenience, the following discussion of the fracture-toughness values and strengths is divided between lay-ups with 0° plies and those without 0° plies.

Lay-ups with 0° plies.- As previously noted, the $[0_2/90/0]_s$, $[0_2/45/0_2/-45/0_2]_s$, and $[90/0]_{2s}$ specimens developed long splits at the slot ends in the 0° plies. The splits elevated the strengths and, consequently, the K_Q values. (See figs. 7 and 8(a) to (c).) Recall that the splits were longest for the $[0_2/90/0]_s$ specimens and shortest for the $[90/0]_{2s}$ specimens. The elevation in K_Q values and strengths varied accordingly. The strengths for many of the $[0_2/90/0]_s$ specimens in figure 8(a) were elevated so much that $S_{net} \approx F_{tu}$. As a result, the mean K_Q value was more than three times the predicted value. Note also the large scatter in the strengths in figures 8(a) to (c) and, correspondingly, the large COV values for K_Q

in figure 8. This variability is probably caused by variability in splitting of the 0° plies. Although the strengths of some $[90/0]_{2s}$ specimens were 50 percent larger than predicted, some were as low as predicted, which indicates that some specimens apparently did not split much at all.

For the other lay-ups with 0° plies, crack-tip damage was relatively small, and the measured and predicted values of K_Q and strength agreed fairly well. (See figs. 7 and 8(d) to (j).) Except for the $[45/0/-45/0]_{2s}$ BP-907 and $[45/0/-45/90]_s$ 5208 lay-ups, the mean values of K_Q in figure 7 are within ±10 percent of the predicted values. For the $[45/0/-45/0]_{2s}$ BP-907 lay-up it is 18 percent below, and for the $[45/0/-45/90]_s$ 5208 lay-up it is 22 percent above. Of course, the strengths show the same difference. A similar trend was found in reference 2.

Although the 0° plies did not split noticeably at the slot ends, the 45° and 90° plies did. However, splitting of the 45° and 90° plies should not elevate strengths as much as splitting of the 0° plies, which are the principal load-carrying plies. The coefficients of variation, which lie between 0.056 and 0.144, are close to that for fiber strengths (0.100). They are smaller for the BP-907 lay-ups than for the corresponding 5208 lay-ups (26 to 37 percent less). Recall from figures 4 and 6 that crack-tip damage was also smaller for the BP-907 matrix than for the weaker 5208 matrix. Thus, the variability in K_Q values increased with crack-tip damage even when the damage was relatively small.

Except for the $[45/0/-45/0]_{Ns}$ lay-ups, the predicted K_Q values in figure 7 were a lower bound for the average measured values. If Q_c/ε_{tuf} was reduced from 1.5 to 1.25 $mm^{1/2}$ in equation (4), the predictions would have been a lower bound for all average measured values. Furthermore, if Q_c/ε_{tuf} was reduced to 1.15 $mm^{1/2}$, the predictions would have been a lower bound for all average measured values less one standard deviation.

Harris and Morris (ref. 6) also found that K_Q was strongly affected by crack-tip damage. For thick T300/5208 laminates, crack-tip damage was small and occurred only in the plies near the surface. The interior plies had little or no damage. Thus, the behavior of the thick laminates was dominated by plies that had little or no damage. For $[0/\pm45/90]_{Ns}$ and $[0/90]_{Ns}$ laminates, K_Q decreased with thickness; but for $[0/\pm45]_{Ns}$, K_Q increased with thickness. Because $[0/\pm45]_{Ns}$ is similar to $[45/0/-45/0]_{Ns}$, the large K_Q values here for $[45/0/-45/90]_s$ and $[90/0]_{2s}$ 5208 laminates and the small K_Q values for $[45/0/-45/0]_{Ns}$ 5208 laminates are consistent with the findings of Harris and Morris. The decrease in K_Q with thickness for $[0/\pm45]_{Ns}$ is unexpected on the basis of crack-tip damage. The cause is not obvious.

Lay-ups without 0° plies.- The ±45° plies are the principal load-carrying plies of the $[90/45/90/-45]_s$ and $[\pm45]_{2s}$ 5208 specimens. Consequently, the large ±45° splits at the crack tips of these specimens elevated strengths much like the large 0° splits in specimens with 0° plies. For this reason, the measured strengths of the 305-mm-wide specimens in figures 9(a) and (b) are greater than the predicted curve. In contrast, the strengths of the 100-mm-wide specimens are closer to the predicted curve, especially those of the $[\pm45]_{2s}$ 5208 specimens. They are closer because the strengths are constrained to lie between the predicted curve and the $S_{net} = F_{tu}$ curve. These curves are much closer together for the 100-mm-wide specimens than for the 305-mm-wide specimens. They virtually coincide for the 100-mm-wide $[\pm45]_{2s}$ 5208 specimens. Thus, the measured and predicted strengths are constrained to agree for the 100-mm-wide $[\pm45]_{2s}$ 5208 specimens, and the agreement is fortuitous. The average K_Q values for the 100- and 305-mm-wide $[\pm45]_{2s}$ 5208 specimens are 1.08

and 1.64 GPa-mm$^{1/2}$, respectively. The elevated value for the 305-mm-wide specimens is more representative of this lay-up than the average of all the specimens in table IV. On the other hand, the average K_Q value for the 305-mm-wide $[90/45/90/-45]_s$ specimens is only 13 percent greater than that for the 100-mm-wide specimens. Thus, the value in table IV is fairly representative for that lay-up.

In contrast to the behavior of the $[\pm45]_{2s}$ 5208 specimens, the $[\pm45]_{2s}$ BP-907 specimens split much less, and the strengths and K_Q were less. Also, the strengths (except for 2a = 5 mm) and K_Q were overpredicted rather than underpredicted. (See figs. 7 and 9(c).) The $[\pm45]_{2s}$ boron/aluminum specimens in reference 1 were similarly overpredicted. (The curves in fig. 10 of ref. 1 were mislabeled. The labels for the top and bottom curves should be reversed.) The stress strain curves for both $[\pm45]_{2s}$ BP-907 and boron/aluminum are very nonlinear, and the failing strains are greater than 8 percent. It was also shown in reference 1 that the strain-intensity factor $K_{Q\varepsilon}$ and the failing strains of all boron/aluminum lay-ups that have nonlinear stress-strain curves could be predicted more accurately than K_Q and the strengths. Therefore, $K_{Q\varepsilon}$ and the failing strains were also predicted here for $[\pm45]_{2s}$ BP-907.

For a uniaxially loaded center-cracked specimen, $\varepsilon_{oc} = S_c/E_y$ and $K_{Q\varepsilon} = K_Q/E_y$ for a linear-elastic material. For E_y = 16.7 GPa and K_Q = 0.928 GPa-mm$^{1/2}$ (tables I and IV, respectively), $K_{Q\varepsilon}$ = 0.0556 mm$^{1/2}$. Values of $K_{Q\varepsilon}$ were computed for each specimen by using equation (1) with K_Q, S_c, and F_{tu} replaced by $K_{Q\varepsilon}E_y$, $\varepsilon_{oc}E_y$, and $\varepsilon_{tu}E_y$, respectively. Because the grips elevated the strain-gauge readings, far-field failing strains ε_{oc} were calculated from the strengths by using the stress-strain curve in figure 10. These values of ε_{oc} and $K_{Q\varepsilon}$ are given in table III(c) for each specimen. The average value of $K_{Q\varepsilon}$ is 0.0540 mm$^{1/2}$, which is within ±3 percent of the predicted value. Therefore, the agreement between measured and predicted $K_{Q\varepsilon}$ values is much better than that between the K_Q values in figure 7.

Failing strains were predicted by using equation (5) with K_Q, S_c, and F_{tu} replaced by $K_{Q\varepsilon}E_y$, $\varepsilon_{oc}E_y$, and $\varepsilon_{tu}E_y$, respectively, and with $K_{Q\varepsilon}$ = 0.0556 mm$^{1/2}$ and ε_{tu} = 0.0871. Strengths were then calculated by using the nonlinear stress-strain curve in figure 10 and plotted in figure 9(c). As expected, the strengths calculated from predicted failing strains are lower than those predicted directly with K_Q. They agree better with the measured strengths for 2a = 20 mm, but not with those for 2a = 5 mm. Although the agreement is better in one case than in the other, the strengths calculated from predicted failing strains are conservative in both cases, whereas those predicted directly with K_Q are not.

Parametric Study of Factors Influencing K_Q

Fiber properties.- When all plies of a laminate are made of one material, the fracture toughness K_Q of the laminate is proportional to fiber strength and does not depend on fiber failing strain. This can be shown relatively easily with equation (4) for lay-ups with $E_x = E_y$ such as quasi-isotropic lay-ups. For this case, $E_y/\xi = E_y(1 - \nu_{yx})$. By using lamination theory to express E_y and ν_{yx} in terms of lamina constants and replacing $E_{11}\varepsilon_{tuf}$ with V_fF_{tuf}, equation (4) can be written as

$$K_Q = 0.75V_f F_{tuf}[E_{11} + E_{22}(1 + 2\nu_{12})]/(E_{11} - \nu_{12}E_{22}) \quad (6)$$

For $E_{22}/E_{11} < 1$, the factor in brackets on the right-hand side of equation (6) is approximately $1 + [(1 + 3\nu_{12})E_{22}/E_{11}]$. Thus, K_Q is proportional to V_f and F_{tuf} and increases approximately linearly with the ratio E_{22}/E_{11} and ν_{12}. For $E_{22}/E_{11} \ll 1$, $K_Q \approx 0.75V_f F_{tuf}$.

Predicted and measured values of K_Q from equation (6) and reference 2, respectively, are plotted in figure 11 for $[0/\pm45/90]_s$ laminates made with five different combinations of fiber and resin matrix materials. The calculations were made by using the properties in table I and in the following table:

Material	E_{11}, GPa	E_{22}, GPa	ν_{12}	G_{12}, GPa	V_f
Boron/epoxy	207	20.7	0.270	7.31	0.45
Celion 6000[5]/polyimide . . .	136	9.31	.357	6.14	.61
E-glass/epoxy	38.6	8.27	.260	4.14	.53

The experimental values of K_Q agree well with equation (6). The curve for boron and graphite is close to that for $E_{22}/E_{11} = 0$, but the curve for E-glass is significantly elevated by a relatively large value of E_{22}/E_{11}. Notice that the laminate with the smallest fiber failing strain (shown in parentheses in figure 11) has the largest K_Q and vice versa.

For lay-ups with 0° plies, laminate strength F_{tu}, like K_Q, is approximately proportional to fiber strength F_{tuf}. Consequently, the ratio K_Q/F_{tu}, which is a measure of notch sensitivity or strength retention, is approximately independent of F_{tuf}. Thus, an increase in fiber strength would increase laminate strength without increasing notch sensitivity. For lay-ups without 0° plies, an increase in fiber strength should also not increase notch sensitivity. In fact, it should increase K_Q without changing F_{tu} and will thus decrease notch sensitivity.

Fiber stiffness, as well as fiber strength, affects K_Q when different kinds of fibers are combined as in a "hybrid" laminate. Consider a hybrid with Du Pont Kevlar 49 or S-glass 0° plies and T300 graphite off-axis plies. These fibers have similar strengths, but T300 graphite fibers are much stiffer than either Kevlar 49 or S-glass fibers. The lamina properties for these fibers in a 5208 epoxy matrix are tabulated as follows:

Material	E_{11}, GPa	E_{22}, GPa	ν_{12}	G_{12}, GPa	ε_{tuf}
T300 graphite/epoxy	129	10.9	0.312	5.65	0.0100
Kevlar 49/epoxy	74.1	5.16	.421	2.07	.0165
S-glass/epoxy	49.4	17.8	.291	4.48	.0271

[5]Celion 6000: Registered trademark of Celanese Corporation.

Values of K_Q were calculated by use of equation (4) for the hybrids and for $[45/0/-45/90]_{2s}$ and $[45/0_2/-45/90]_{2s}$ epoxy lay-ups made with all T300 graphite, all Kevlar 49, and all S-glass plies. For the hybrid laminates, the failing strain of the 0° fibers was used for ε_{tuf} in equation (4). The laminate constants were calculated from the lamina constants by using lamination theory. The values of laminate constants and K_Q are given in table VI.

The predicted K_Q values are plotted in figure 12 for the $[45/0/-45/90]_{2s}$ lay-ups. For the lay-ups of one material (open bars), notice that K_Q for S-glass is about 50 percent greater than that for T300 graphite and Kevlar 49, even though fiber strengths are nearly equal. They differ because E_{22}/E_{11} for S-glass is four times that for T300 graphite and Kevlar 49. (Recall that K_Q increases linearly with E_{22}/E_{11} for this lay-up.) For the hybrids, the combination of fibers affects K_Q synergistically. For the S-glass hybrid (and similarly for the Kevlar 49 hybrid), K_Q is larger than that for the lay-ups of either all S-glass or all T300 graphite. Thus, K_Q is larger when the off-axis plies are stiffer than the 0° plies. The increase in laminate stiffness produces this effect by reducing strains in the principal load-carrying plies for a given applied stress. The increase in K_Q with E_{22}/E_{11} is produced the same way.

Experimental results for the hybrids (ref. 7) and for the lay-up of all T300 graphite (table IV) are plotted in figure 12 for comparison. Only the results for the widest (101.4 mm) hybrid specimens in reference 7 are plotted. The strengths of the narrower specimens are lower because the strengths are limited by large net-section stresses ($S_{net} \approx F_{tu}$). The experiments and predictions agree quite well.

The predicted K_Q values for the $[45/0_2/-45/90]_{2s}$ lay-ups are shown in figure 13. The values for $[45/0/-45/90]_{2s}$ are included for comparison. For each $[45/0_2/-45/90]_{2s}$ lay-up, the predicted value of K_Q is only slightly larger than that for the corresponding $[45/0/-45/90]_{2s}$ lay-up. The difference is less than 20 percent. The trends for the two lay-ups are the same. The experimental values for the 101.6-mm-wide $[45/0_2/-45/90]_{2s}$ specimens from reference 7 are shown for comparison. In the $[45/0_2/-45/90]_{2s}$ specimens, the 0° plies split extensively at the slot ends and the experimental K_Q values were greatly elevated, particularly for the Kevlar 49 hybrid.

Matrix properties.- Recall that the value of Q_c was shown to be $1.5\varepsilon_{tuf}$ $mm^{1/2}$ for all fibrous composite materials with small crack-tip damage (ref. 2). For T300 fibers with $\varepsilon_{tuf} = 0.010$, $Q_c = 0.015$ $mm^{1/2}$ regardless of matrix properties and fiber volume fraction. To verify this, Q_c values were calculated for the BP-907 and corresponding 5208 lay-ups and plotted in figure 14 for comparison. For the $[45/0/-45/90)_{Ns}$ and $[45/0/-45/0]_{Ns}$ lay-ups, $Q_c = \xi K_Q/E_y$ was calculated by using the average values of K_Q in table IV. For the $[\pm45]_{2s}$ BP-907 lay-up, $Q_c = \xi K_{Q\varepsilon}$ was calculated by using $K_{Q\varepsilon} = 0.0540$ $mm^{1/2}$, which was the average of the $K_{Q\varepsilon}$ values in table III(c); and for $[\pm45]_{2s}$ 5208, $Q_c = \xi K_Q/E_y$ was calculated by using $K_Q = 1.64$ GPa-$mm^{1/2}$, which was the average of the K_Q values for the 305-mm-wide specimens in table II(j). As noted previously, these calculations give better estimates of Q_c for the $[\pm45]_{2s}$ lay-ups than those calculated with the mean values of K_Q in table IV. All calculations were made with the E_y and ξ values in table I.

Also for comparison, the measured and predicted strengths of the 5208 and BP-907 specimens are plotted against slot length in figure 15. Each symbol represents an average strength for a given slot length and specimen width. The strengths for 100-mm-wide 5208 specimens, which failed at $S_{net} = F_{tu}$, are not plotted in

figure 15(c). The strengths are multiplied by the finite-width correction factor as before. The BP-907 strengths are also multiplied by the ratios of V_f for the corresponding 5208 and BP-907 lay-ups to eliminate the effect of differences between V_f values. The strengths of the specimens were predicted as before. For the $[\pm 45]_{2s}$ BP-907 specimens, the strengths calculated from predicted failing strains were plotted rather than those predicted directly.

For the $[45/0/-45/90]_{Ns}$ and $[45/0/-45/0]_{2s}$ lay-ups, the F_{tu} and predicted K_Q values for BP-907 and 5208 are nearly equal when adjusted for the differences in fiber volume fractions. Consequently, the predicted values of strength for BP-907 and 5208 are virtually equal and are represented by a single curve in figures 15(a) and (b). Even though the measured values of Q_c and the strength for 5208 are slightly larger than those for BP-907, they still agree well with the predictions. Recall that crack-tip damage, albeit relatively small, was also larger for the 5208 lay-ups.

The K_Q (and thus Q_c) values of the $[45/0/-45/90]_s$ and $[45/0/-45/0]_{2s}$ 5208 specimens also increase somewhat with slot length. (See the Q_c values in fig. 16.) The other 5208 lay-ups exhibit this same trend, as seen in table II. (Many other investigators have noted a similar behavior.) This increase is especially noticeable for the $[0_2/90/0]_s$, $[0_2/45/0_2/-45/0_2]_s$, and $[90/0]_{2s}$ specimens, which developed splits in the 0° plies at the slot ends. The Q_c values for the BP-907 specimens, which are also plotted in figure 16, do not exhibit this trend up to the longest slots tested. Thus, the evidence here indicates that crack-tip damage causes K_Q to increase with crack length. Furthermore, the average Q_c values for 5208 in figure 14 are biased toward short slots, which are the most numerous. For this reason, the agreement between Q_c values for 5208 and BP-907 may be limited to short slots. The difference between these epoxies may be more important for long slots.

For the $[\pm 45]_{2s}$ lay-ups, the predicted values of strength for BP-907 and 5208 in figure 15(c) are equal for long slots but not for short slots. The predicted K_Q values are virtually equal when adjusted for the difference between fiber volume fractions, but the adjusted value of F_{tu} for BP-907 is about 1.5 times that for 5208. Consequently, when the slots are small, the predicted values of adjusted strengths for BP-907 are larger than those for 5208. As slot length increases, the curves cross because of the nonlinear stress-strain behavior of $[\pm 45]_{2s}$ BP-907 and merge for long slots as the strengths approach $K_Q(\pi a)^{-1/2}$. The measured values of strength and Q_c for 5208 are much greater than the predicted values because of the extensive splitting noted previously; on the other hand, those for the stronger BP-907 matrix, which split much less, are smaller and agree with the predictions.

Therefore, when lay-ups tend to split at the crack tips, an increase in matrix strength reduces K_Q and thus increases notch sensitivity. For angle-ply lay-ups like $[\pm 45]_{2s}$, failure of uncracked specimens is via the matrix, and an increase in matrix strength also increases F_{tu}. (In table I, F_{tu} is 24 percent greater for $[\pm 45]_{2s}$ BP-907 than for $[\pm 45]_{2s}$ 5208.) Consequently, an increase in matrix strength can increase the notch sensitivity of angle-ply lay-ups even when they do not split at the crack tips.

Matrix stiffness also affects K_Q through the elastic constants E_x, E_y, and ν_{yx}. (Recall that $K_Q = 1.5\varepsilon_{tuf}E_y/\xi$.) However, for different resin matrices, the elastic constants and, consequently, K_Q are usually not much different for a given fiber volume fraction. Such is the case for 5208 and BP-907. Even differences

between the elastic constants for metal and resin matrices will not greatly affect K_Q (ref. 2). Thus, for lay-ups that tend to split at the crack tips, matrix strength affects K_Q much more than matrix stiffness.

Lay-up.- The dependence of K_Q on lay-up is shown in the Cordell graph (ref. 8) in figure 17. Here, values of K_Q predicted by equation (4) for T300/5208 are plotted against the proportion of 0°, ±45°, and 90° plies. Splitting at the crack tips is, of course, not taken into account. Two surfaces are predicted - one for 0° principal load-carrying plies and one for 45° plies. (A surface is not shown for 90° plies since ε_1 is not critical for these plies.) The two surfaces intersect along the line for which $E_x = E_y$. Here, also, K_Q is a constant. The surface for 45° plies will govern only in the foreground of the graph, in which the proportion of 0° plies is zero or very small.

The surfaces in figure 17 are inclined so that K_Q increases with the proportion of 0° plies whenever the proportion of 45° or 90° plies are held constant. However, K_Q does not increase with the proportion of 0° plies in other cases. For example, along the line $E_x = E_y$, the proportion of 0° plies varies from 0 for the [±45] lay-up to 50 percent for the [0/90] lay-up, and K_Q is constant. (Recall that the predicted K_Q value in table IV for the $[\pm 45]_{2s}$, $[45/0/-45/90]_s$, and $[90/0]_{2s}$ 5208 lay-ups is 1.11 GPa-mm$^{1/2}$.) Moreover, the surfaces in figure 17 are tilted so that K_Q can even decrease as the proportion of 0° plies increases.

Several researchers have reported that K_Q increases with F_{tu} (refs. 9, 10, and 11). For lay-ups with 0° plies, replacing $\varepsilon_{tuf}E_y$ in equation (4) with F_{tu} gives

$$K_Q = 1.5F_{tu}/\xi$$

Thus, according to this equation, K_Q is not only proportional to F_{tu} but it also varies inversely with ξ. Since ξ and F_{tu} vary with lay-up, K_Q does not necessarily increase in proportion to F_{tu}.

To show how K_Q varies with F_{tu}, numerous planes were passed through the surface for 0° principal load-carrying plies ($\alpha^* = 0°$) in figure 17. Values of F_{tu} were calculated by using $\varepsilon_{tuf}E_y$. The results are plotted in figure 18. The curve for $\lambda = 0$ was calculated for $\alpha^* = 0°$ and is thus hypothetical. It represents the limit for a small number of 0° plies. The K_Q values predicted for $[\pm 45]_{2s}$ and $[90/45/90/-45]_s$ lay-ups assuming $\alpha = 45°$ are plotted as symbols against actual F_{tu} values. They are close to the $\lambda = 0$ curve.

The results indicate that K_Q and F_{tu} are not uniquely related, although K_Q does, in general, increase with F_{tu}. Notice that they are approximately proportional for $[0_m/90_p]_s$ lay-ups. Values of K_Q are largest for $[0_m/\pm 45_n]_s$ lay-ups and smallest for $[0_m/90_p]_s$ lay-ups. The values for $[\pm 45]_{2s}$ and $[90/45/90/-45]_s$ lay-ups are to the left of the $\lambda = 0$ curve. For lay-ups with $E_x = E_y$, F_{tu} varies from 160 MPa for $[\pm 45]_s$ to 705 MPa for $[0/90]_s$, even though K_Q is constant. On the other hand, for lay-ups with a constant proportion of 0° plies, F_{tu} is more nearly constant but K_Q increases dramatically with the proportion of 45° plies. For a given proportion of 0° plies, the most notch-sensitive lay-ups (smallest ratio of K_Q to F_{tu}) are $[0_m/90_p]_s$, and the least sensitive are $[0_m/\pm 45_n]_s$. Notice that

lay-ups with $E_x = E_y$ have the greatest range of notch sensitivity. The $[\pm 45]_{2s}$ lay-up is the least notch sensitive.

Recall that the $[0]_{8T}$, $[0_2/90/0]_s$, $[0_2/45/0_2/-45/0_2]_s$, and $[90/0]_{2s}$ specimens split extensively at the crack tips. The $[0]_{8T}$ specimens for both BP-907 and 5208 split from the crack tips to the grips before the intact ligaments failed at $S_{net} = F_{tu}$. Some $[0_2/90/0]_s$ specimens split to the grips also. Even when the splits did not extend to the grips, K_Q values were 50 to 250 percent greater than those predicted in figure 18. (See fig. 7.) Therefore, the notch sensitivity of these lay-ups is greatly exaggerated in figure 18. However, extensive splitting at the crack tips is actually a longitudinal failure and is not acceptable in most applications. Thus, lay-ups that split extensively when notched have few applications. Laminates will be made with matrix materials that are strong enough to prevent or limit crack-tip damage like splitting and will therefore have K_Q values near those predicted with $K_Q = 1.5\varepsilon_{tuf}E_y/\xi$. For example, unidirectional boron/aluminum, which has application in tubes, does not split like unidirectional lay-ups with conventional epoxies. The $[0]_{6T}$ boron/aluminum specimens in reference 1 failed in a self-similar manner near the predicted K_Q value.

For metals, crack-tip yielding elevates K_Q much like crack-tip splitting for the composites here. To assure minimum or valid K_Q values for metals, the size of the yield zone is restricted to be small compared to the specimen thickness. The size of the yield zone is predicted by using the singular stress field with a maximum-stress criterion. Minimum K_Q values for composites could be assured similarly by restricting split length to be much less than crack length. Equation (13) in the appendix can be used to predict the split length for epoxy matrices. However, it will greatly overpredict split length for metal matrices that behave more like elastic perfectly plastic materials.

Up to this point, only $[0_m/\pm 45_n/90_p]_s$ lay-ups have been considered. Another important family of lay-ups, $[0_m/\pm\alpha_n]_s$, will be analyzed here for completeness. Filament-wound and angle-ply $[\pm\alpha]_s$ lay-ups belong to this family. (Although filament-wound lay-ups are generally not symmetric, the results for symmetric lay-ups are reasonably accurate for axisymmetric pressure vessels.)

Values of K_Q predicted by equation (4) for $\alpha^* = 0°$ are shown in figure 19 for $[0_m/\pm\alpha_n]_s$ lay-ups with various angles α and proportions of 0° plies λ. The predictions were made with laminate constants that were calculated by using lamina constants and lamination theory. The elastic constants for $[0]_{8T}$ T300/5208 in table I were used for the lamina constants. A 1-percent failing strain was used for ε_{tuf}. As before, splitting is not taken into account.

The value of K_Q in figure 19 decreases with α and increases with λ. For $\lambda = 0$, two curves are shown - one for $\alpha^* = 0°$ and one for $\alpha^* = \alpha$ (angle-ply lay-ups). The curve for $\alpha^* = 0°$ is hypothetical, of course, and represents the limit as λ becomes small. The 0° plies can be critical for small λ when α is large because the strength of angle plies decreases dramatically with increasing α (ref. 12). For $\alpha > 60°$, the strength ratio of α plies to 0° plies is less than 0.05.

For angle-ply lay-ups with large α, failure tends to be via matrix and not fiber (refs. 12 and 13). Thus, the angle-ply curve in figure 19 will be overpredicted for a large α. Recall that K_Q for the narrow $[\pm 45]_{2s}$ 5208 specimens was limited by the restriction $S_{net} \leq F_{tu}$.

To show notch sensitivity for $[0_m/\pm\alpha_n]_s$, the predicted values of K_Q are plotted against F_{tu} in figure 20 for the various values of α and λ. For the $[\pm45]_{2s}$ angle-ply lay-ups, measured F_{tu} values in table I were plotted; and for $[\pm\alpha]$, those in reference 12 were plotted. (The angle-ply curve was not plotted for $\lambda > 60°$.) For the lay-ups with various proportions of 0° plies, values of $F_{tu} = 0.010E_y$ were plotted. The curve for $[0_m/90_n]_s$ is a lower bound for $[0_m/\pm\alpha_n]_s$ lay-ups as well as for $[0_m/\pm45_n/90_p]_s$ lay-ups. The curve for $\lambda = 0$ is an upper bound except for angle-ply lay-ups with $\alpha > 45°$. The curves for $\alpha > 45°$ are even above the curve for $[0_m/\pm45_n]_s$. Thus, the range of K_Q values for $[0_m/\pm\alpha_n]_s$ lay-ups is greater than that for $[0_m/\pm45_n/90_p]_s$ lay-ups.

For a given angle α, the notch sensitivity of all $[0_m/\pm\alpha_n]_s$ lay-ups (including angle ply) increases with λ. The curve for $\lambda = 0$ does not represent the least notch-sensitive lay-ups even though it is an upper bound for K_Q. The least notch-sensitive lay-ups are defined by a locus of points for which a line through the origin is tangent to a λ = Constant curve. This locus of points happens to coincide approximately with the angle-ply curve. The angle α varies between 40° and 45°, depending on λ. Thus, for a given λ, the least notch-sensitive $[0_m/\pm\alpha_n]_s$ lay-ups have $40° \leq \alpha \leq 45°$. For $\alpha < 40°$, notch sensitivity decreases with increasing α; and for $\alpha > 45°$, it increases with increasing α.

Recall that $[0_m/\pm45_n]_s$ is also the least notch sensitive of all $[0_n/\pm45_n/90_p]_s$ lay-ups. Therefore, for a given proportion of 0° plies, the least notch sensitive of all $[0_m/\pm\alpha_n]_s$ and $[0_m/\pm45_n/90_p]_s$ lay-ups is, for all intents and purposes, $[0_m/\pm45_n]_s$. (Splitting, of course, could make other lay-ups less notch sensitive.)

It was noted in the previous section that an increase in matrix strength increased the notch sensitivity of $[\pm45]_{2s}$ lay-ups whether or not crack-tip splits develop. This should be true of all angle-ply lay-ups, except $\alpha = 0°$, as long as $S_{net} < F_{tu}$.

Equation (4) predicts two important characteristics for quasi-isotropic lay-ups that do not split at the crack tips. These lay-ups include all balanced and symmetric lay-ups with ply angles of 0°, π/N_o, $2\pi/N_o$, $(N_o - 1)\pi/N_o$, ..., where $N_o \geq 3$. First, since K_Q is a constant for all lay-ups with $E_x = E_y$, K_Q is a constant for all quasi-isotropic lay-ups, for example, $[0/\pm60]_s$, $[0/\pm45/90]_s$, $[0/\pm36/\pm72]_s$, and so forth. Second, since the elastic constants are invariant, E_y/ξ and, consequently, K_Q are invariant. Thus, in a quasi-isotropic laminate, K_Q is uniform in all directions parallel to the plane of the laminate, as are the elastic constants. These predictions for quasi-isotropic lay-ups will, of course, be valid only when the crack-tip damage is nonexistent or very small. Otherwise, K_Q may not be quasi-isotropic. For example, crack-tip damage may be different between $[0/\pm60]_s$ and $[90/\pm30]_s$. Consequently, actual K_Q values may be different. (Uncracked strengths are different for $[0/\pm60]_s$ and $[90/\pm30]_s$. The $[0/\pm60]_s$ fails via fibers and the $[90/\pm30]_s$ fails via matrix.)

CONCLUSIONS

The fracture toughness K_Q of T300/5208 and T300/BP-907 laminates with various proportions of 0°, ±45°, and 90° plies was determined by testing center-cracked specimens. It was also predicted with the general fracture-toughness parameter. The following conclusions were reached:

1. Predictions were good except when lay-ups tended to develop large crack-tip damage like splitting.

2. The propensity to split can be predicted.

3. With large crack-tip damage, the strengths and K_Q values were elevated.

4. Strong, tough matrices, which allow little or no crack-tip damage, give minimum K_Q values.

Predictions were also made for $[0_m/\pm45_n/90_p]_s$ and $[0_m/\pm\alpha_n]_s$ lay-ups to determine how fiber and matrix properties as well as lay-up affect K_Q. When failure was via fibers without crack-tip splitting, the following conclusions were reached:

1. The K_Q increases in proportion to fiber strength and fiber volume fraction.

2. The K_Q increases linearly with E_{22}/E_{11}. (The E_1 and E_2 are Young's moduli of the lamina parallel to and normal to the direction of the fibers, respectively.)

3. The K_Q is larger when the modulus of non-0° fibers is greater than that of 0° fibers.

4. The K_Q is lowest for $[0_m/90_p]_s$ lay-ups.

5. The K_Q and ultimate tensile strength of a laminate are not uniquely related and, in general, do not increase proportionately.

6. The K_Q is the same for all lay-ups with $E_x = E_y$. (The E_x and E_y are the Young's moduli of the laminate parallel to and normal to the slot or crack, respectively.

7. For a given proportion of 0° plies, the most notch-sensitive lay-ups are $[0_m/90_p]_s$ and the least sensitive are $[0_m/\pm45_n]_s$ and $[\pm\alpha]_s$.

8. Notch sensitivity increases with the proportion of 0° plies and, for $[\pm\alpha]_s$, decreases with α.

Langley Research Center
National Aeronautics and Space Administration
Hampton, VA 23665
August 31, 1984

APPENDIX

SPLITTING PREDICTIONS

The length of splits in the various plies of the laminates can be predicted by using the singular stress field from the theory of elasticity and the Tsai-Hill failure criterion. By using the notation in reference 5, the lamina strains in a ply with angle α are given by

$$\begin{Bmatrix} \varepsilon_1 \\ \varepsilon_2 \\ \frac{1}{2}\gamma_{12} \end{Bmatrix}_\alpha = [T]_\alpha [B] \begin{Bmatrix} \sigma_x \\ \sigma_y \\ \tau_{xy} \end{Bmatrix} \tag{7}$$

where the transformation matrix is

$$[T]_\alpha = \begin{bmatrix} \sin^2 \alpha & \cos^2 \alpha & \sin 2\alpha \\ \cos^2 \alpha & \sin^2 \alpha & -\sin 2\alpha \\ -\frac{1}{2}\sin 2\alpha & \frac{1}{2}\sin 2\alpha & -\cos 2\alpha \end{bmatrix}$$

and the matrix of laminate constants is

$$[\beta] = \begin{bmatrix} \frac{1}{E_x} & -\frac{\nu_{xy}}{E_x} & 0 \\ -\frac{\nu_{yx}}{E_y} & \frac{1}{E_y} & 0 \\ 0 & 0 & \frac{1}{2G_{xy}} \end{bmatrix}$$

Plane-stress conditions were assumed. The lamina stresses in the α ply are given by

$$\begin{Bmatrix} \sigma_1 \\ \sigma_2 \\ \tau_{12} \end{Bmatrix}_\alpha = [Q] \begin{Bmatrix} \sigma_1 \\ \varepsilon_2 \\ \frac{1}{2}\gamma_{12} \end{Bmatrix}_\alpha \tag{8}$$

where

$$[Q] = \begin{bmatrix} \dfrac{E_{11}}{1 - \nu_{12}\nu_{21}} & \dfrac{\nu_{21}E_{11}}{1 - \nu_{12}\nu_{21}} & 0 \\ \dfrac{\nu_{12}E_{22}}{1 - \nu_{12}\nu_{21}} & \dfrac{E_{22}}{1 - \nu_{12}\nu_{21}} & 0 \\ 0 & 0 & 2G_{12} \end{bmatrix}$$

σ_1 and σ_2 are the normal stresses parallel to and perpendicular to the fibers, respectively, and τ_{12} is the corresponding shear stress.

For a specially orthotropic plate with a cracklike slot and remote uniaxial stress, the theory of elasticity gives the singular laminate stresses (ref. 14) along $\theta = \alpha$ as

$$\begin{Bmatrix} \sigma_x \\ \sigma_y \\ \tau_{xy} \end{Bmatrix} = K(2\pi r)^{-1/2}\{D\} \tag{9}$$

where

$$\{D\} = \begin{Bmatrix} \mathrm{Re}\left[\dfrac{\mu_1\mu_2}{\mu_1 - \mu_2}(H_2\mu_2 - H_1\mu_1)\right] \\ \mathrm{Re}\left[\dfrac{1}{\mu_1 - \mu_2}(H_2\mu_1 - H_1\mu_2)\right] \\ \mathrm{Re}\left[\dfrac{\mu_1\mu_2}{\mu_1 - \mu_2}(H_1 - H_2)\right] \end{Bmatrix}$$

$$H_1 = (\sin\alpha + \mu_1\cos\alpha)^{-1/2}$$

and

$$H_2 = (\sin\alpha + \mu_2\cos\alpha)^{-1/2}$$

and the real part of the complex expression is denoted by Re. The μ_1 and μ_2 are two complex roots of the characteristic equation (ref. 14). (The $\bar{\mu}_1$ and $\bar{\mu}_2$ are the other two complex roots where $\bar{\mu}_1$ and $\bar{\mu}_2$ are the complex conjugates of μ_1 and μ_2, respectively.) For $C_2 \geq 1$,

$$\mu_1 = i\left\{C_1\left[C_2 - \left(C_2^2 - 1\right)^{1/2}\right]\right\}^{1/2}$$

$$\mu_2 = i\left\{C_1\left[C_2 + \left(C_2^2 - 1\right)^{1/2}\right]\right\}^{1/2}$$

and for $-1 < C_2 \leq 1$,

$$\mu_1 = \left[\frac{C_1(1 - C_2)}{2}\right]^{1/2} + i\left[\frac{C_1(1 + C_2)}{2}\right]^{1/2}$$

$$\mu_2 = -\left[\frac{C_1(1 - C_2)}{2}\right]^{1/2} + i\left[\frac{C_1(1 + C_2)}{2}\right]^{1/2}$$

where

$$C_1 = \left(\frac{E_x}{E_y}\right)^{1/2}$$

and

$$C_2 = C_1\left(\frac{E_y}{2G_{xy}} - \nu_{yx}\right)$$

Materials cannot have $C_2 < -1$ (real μ_1 and μ_2).

Combining equations (7), (8), and (9) gives

$$\begin{Bmatrix}\sigma_1\\ \sigma_2\\ \tau_{12}\end{Bmatrix}_\alpha = \frac{K}{(2\pi r)^{1/2}}\begin{Bmatrix}M_1\\ M_2\\ M_{12}\end{Bmatrix}_\alpha \qquad (10)$$

where

$$\begin{Bmatrix} M_1 \\ M_1 \\ M_{12} \end{Bmatrix}_\alpha = [Q][T]_\alpha[\beta]\{D\}$$

The Tsai-Hill failure criterion (ref. 5) is

$$\left(\frac{\sigma_{1m}}{\sigma_{1mu}}\right)^2 + \left(\frac{\sigma_2}{\sigma_{2u}}\right)^2 - \left(\frac{\sigma_{2u}}{\sigma_{1mu}}\right)\left(\frac{\sigma_{1m}}{\sigma_{1mu}}\right)\left(\frac{\sigma_2}{\sigma_{2u}}\right) + \left(\frac{\tau_{12}}{\tau_{12u}}\right)^2 = 1 \tag{11}$$

where σ_{1mu}, σ_{2u}, and τ_{12u} are the allowables for σ_{1m}, σ_2, and τ_{12}, respectively, and

$$\sigma_{1m} = \sigma_1 E_m / E_{11} \tag{12}$$

where E_m is Young's modulus of the neat resin. For both 5208 and BP-907 resins, E_m was assumed equal to 3.5 GPa. The matrix stress σ_{1m} was used in equation (11) rather than σ_1 because the failure with σ_1 acting alone is via fiber and not matrix. Thus, the use of σ_1 (stress in fiber) in equation (11) would be inappropriate for predicting split length. (Splitting is matrix failure.) Equation (12) is exact only for a state of uniaxial stress. The error in its use here is not believed to be significant.

Substituting equations (10) and (12) into (11), replacing K by K_Q and r by ℓ_α, and solving for ℓ_α gives

$$\ell_\alpha = \ell_{1\alpha} + \ell_{2\alpha} - \frac{\sigma_{2u}}{\sigma_{1mu}}(\ell_{1\alpha}\,\ell_{2\alpha})^{1/2} + \ell_{12\alpha} \tag{13}$$

where

$$\ell_{1\alpha} = \frac{K_Q^2}{2\pi}\left(\frac{M_1}{\sigma_{1mu}}\right)_\alpha^2$$

$$\ell_{2\alpha} = \frac{K_Q^2}{2\pi}\left(\frac{M_2}{\sigma_{2u}}\right)_\alpha^2$$

and

$$\ell_{12\alpha} = \frac{K_Q^2}{2\pi}\left(\frac{M_{12}}{\tau_{12u}}\right)_\alpha^2$$

In equation (13), ℓ_α corresponds to the split length in the ply with angle α when the specimen fails and $\ell_{1\alpha}$, $\ell_{2\alpha}$, and $\ell_{12\alpha}$ are contributions from σ_{1m}, σ_2, and τ_{12}, respectively. Also, $\ell_{1\alpha}$, $\ell_{2\alpha}$, and $\ell_{12\alpha}$ correspond to split lengths given by maximum-stress criteria. The calculations of ℓ_α were made with the elastic constants in table I, the values of σ_{1mu}, σ_{2u}, and τ_{12u} in table VII, and the predicted values of K_Q. For all the lay-ups in table I, σ_1 and σ_2 given by equation (10) are tension.

The allowables in table VII were determined as follows. The values of τ_{12u} were calculated as one-half the tensile strengths of the $[\pm45]_{2s}$ lay-ups in table I. Neat-resin strengths (ref. 3) were used for σ_{1mu}, and in situ strengths of 90° plies were used for σ_{2u}. The values of σ_{2u} for 5208 were determined from tensile tests of the various lay-ups (ref. 4). They were calculated for the 90° plies at failure, in which failure was indicated by deviations in the tangent modulus of the stress-strain curves. Notice that the resulting σ_{2u} values decrease with the number of contiguous 90° plies and vary with their location. The strength of one 90° surface ply or one or two 90° interior plies is as large as that of the neat resin. However, the strength of four 90° interior plies or two 90° surface plies is as small as that of $[90]_{8T}$. For BP-907, tensile-test data were available only for the neat resin and $[90]_{8T}$. The ratio of σ_{2u} for neat resin to σ_{2u} for $[90]_{8T}$ is about the same for BP-907 as for 5208. Therefore, the σ_{2u} values for the other BP-907 lay-ups were calculated from the neat-resin strength by using the strength ratios for the 5208 lay-ups as factors.

Typical σ_2 and τ_{12} stress-strain curves for BP-907 and 5208 lamina are plotted in figure 21 for comparison. The σ_2 curves were determined from tensile tests of $[90]_{8T}$ specimens; and the τ_{12} curves, from tensile tests of $[\pm45]_{2s}$ specimens.

REFERENCES

1. Poe, C. C., Jr.; and Sova, J. A.: Fracture Toughness of Boron/Aluminum Laminates With Various Proportions of 0° and ±45° Plies. NASA TP-1707, 1980.

2. Poe, C. C., Jr.: A Unifying Strain Criterion for Fracture of Fibrous Composite Laminates. Eng. Fract. Mech., vol. 17, no. 2, 1983, pp. 153-171.

3. Williams, Jerry G.; and Rhodes, Marvin D.: The Effect of Resin on the Impact Damage Tolerance of Graphite-Epoxy Laminates. NASA TM-83213, 1981.

4. Garber, D. P.: Tensile Stress-Strain Behavior of Graphite/Epoxy Laminates. NASA CR-3592, 1982.

5. Ashton, J. E.; Halpin, J. C.; and Petit, P. H.: Primer on Composite Materials: Analysis. Technomic Pub. Co., Inc., c.1969.

6. Harris, C. E.; and Morris, D. H.: Fracture Behavior of Thick, Laminated Graphite/Epoxy Composites. NASA CR-3784, 1984.

7. Kennedy, John M.: Fracture Behavior of Hybrid Composite Laminates. A Collection of Technical Papers, Part 1: Structures and Materials - AIAA/ASME/ASCE/AHS 24th Structures, Structural Dynamics and Materials Conference, May 1983, pp. 68-73. (Available as AIAA-83-0804.)

8. Cordell, Tobey M.: The Cordell Plot: A Way To Determine Composite Properties. SAMPE J., vol. 13, no. 6, Nov./Dec. 1977, pp. 14-19.

9. Avery, J. G.; and Porter, T. R.: Comparisons of the Ballistic Impact Response of Metals and Composites for Military Aircraft Applications. Foreign Object Impact Damage to Composites, ASTM STP 568, American Soc. Testing & Mater., c.1975, pp. 3-29.

10. Wells, J. K.; and Beaumont, P. W. R.: Correlations for the Fracture of Composite Materials. Scr. Metall., vol. 16, Jan. 1982, pp. 99-103.

11. Caprino, G.; Halpin, J. C.; and Nicolais, L.: Fracture Mechanics in Composite Materials. Composites, vol. 10, no. 4, Oct. 1979, pp. 223-227.

12. Kim, R. Y.: On the Off-Axis and Angle-Ply Strength of Composites. Test Methods and Design Allowables for Fibrous Composites, C. C. Chamis, ed., ASTM STP 734, American Soc. Testing & Mater., c.1981, pp. 91-108.

13. Konish, H. J., Jr.; Cruse, T. A.; and Swedlow, J. L.: Method for Estimating Fracture Strength of Specially Orthotropic Composite Laminates. Analysis of the Test Methods for High Modulus Fibers and Composites, ASTM Spec. Tech. Publ. 521, 1973, pp. 133-142.

14. Paris, Paul C.; and Sih, George C.: Stress Analysis of Cracks. Fracture Toughness Testing and Its Applications, STP No. 381, American Soc. Test. & Mater., c.1965, pp. 30-81.

TABLE I.- LAMINATE PROPERTIES

Laminate	E_y, GPa	E_x, GPa	ν_{yx}	G_{xy}, GPa	ξ	F_{tu} (and $E_y\varepsilon_{tuf}$), MPa	ε_{tu}	V_f
T300/5208								
$[0]_{8T}$	129	10.9	0.312	5.65	0.910	1230 (1290)	0.00902	0.629
$[0_2/90/0]_s$	100	40.7	.0836	5.65	.947	1070 (1000)	.0101	.628
$[0_2/45/0_2/-45/0_2]_s$	103	17.9	.551	12.7	.770	1050 (1030)	.00949	.632
$[90/0]_{2s}$	70.5	70.5	.0482	5.65	.952	667 (705)	.00896	.627
$[90/0/90/0/45/0/-45/0]_s$	76.4	47.4	.214	12.7	.831	782 (764)	.00980	.638
$[45/0/-45/0]_s$	75.3	23.3	.649	19.7	.639	607 (753)	.00769	.650
$[45/0/-45/0]_{2s}$	75.3	23.3	.649	19.7	.639	754 (753)	.00961	.622
$[\pm45/0/\pm45/0]_s$	50.0	25.6	.698	26.0	.501	498 (500)	.0102	.626
$[45/0/-45/90]_s$	51.4	51.4	.307	19.7	.693	396 (514)	.00855	.634
$[90/45/90/-45]_s$	23.3	75.3	.201	19.7	.497	176	.0104	.663
$[\pm45]_{2s}$	19.6	19.6	.735	33.7	.265	160	.0127	.650
T300/BP-907								
$[0]_{8T}$	109	8.32	0.314	4.82	0.913	1330 (1090)	0.0116	0.544
$[45/0/-45/0]_{2s}$	63.4	19.2	.654	16.5	.642	667 (634)	.0109	.552
$[45/0/-45/90]_{2s}$	43.1	43.1	.303	16.5	.697	453 (431)	.0106	.531
$[\pm45]_{2s}$	16.7	16.7	.730	28.2	.270	198	.0871	.540

TABLE II.- FRACTURE DATA FOR T300/5208 LAY-UPS

(a) $[0_2/90/0]_s$

Crack length, 2a, mm	Strength, S_c, MPa	$\frac{S_{net}}{F_{tu}}$	Fracture toughness, K_Q, GPa-mm$^{1/2}$
W = 100 mm			
10.2	763	0.850	4.77
	774	.862	4.94
	617	.687	3.16
20.3	755	0.947	6.88
	544	.682	3.80
	691	.867	5.66
	616	.773	4.59
30.5	441	0.635	3.66
	641	.922	6.42
	633	.911	6.27
	628	.904	6.17
50.8	435	0.884	5.44
	385	.783	4.64
	451	.917	5.72
	411	.835	5.04
W = 305 mm			
30.5	661	0.734	6.15
61.0	593	.741	7.47
91.4	606	.866	10.00
152.4	(a)		

[a]0° plies split to ends and slipped in grips.

(b) $[0_2/45/0_2/-45/0_2]_s$

Crack length, 2a, mm	Strength, S_c, MPa	$\frac{S_{net}}{F_{tu}}$	Fracture toughness, K_Q, GPa-mm$^{1/2}$
W = 100 mm			
10.2	627	0.678	3.20
	591	.639	2.92
	504	.545	2.34
	513	.555	2.39
20.3	427	0.520	2.73
	546	.665	3.77
	425	.518	2.72
	496	.604	3.30
30.5	506	0.707	4.36
	390	.545	3.13
	365	.510	2.90
	451	.630	3.74
50.8	308	0.608	(a)
	306	.604	3.51
	266	.525	2.99
	291	.574	3.31
W = 305 mm			
30.5	400	0.431	3.03
61.0	432	.524	4.80
91.4	385	.534	(b)
152.4	186	.361	(b)

[a]0° plies split to grips.
[b]Specimen failed in grip.

TABLE II.- Continued

(c) $[90/0]_{2s}$

Crack length, 2a, mm	Strength, S_c, MPa	$\frac{S_{net}}{F_{tu}}$	Fracture toughness, K_Q, GPa-mm$^{1/2}$
W = 100 mm			
10.2	286	0.452	1.26
	243	.384	1.04
	319	.504	1.44
	325	.513	1.48
20.3	275	0.489	1.74
	189	.336	1.14
	204	.363	1.24
	212	.377	1.29
30.5	208	0.425	1.61
	170	.347	1.29
	164	.335	1.25
	240	.490	1.89
50.8	143	0.412	1.57
	119	.343	1.30
	110	.317	1.20
	141	.406	1.55
W = 305 mm			
30.5	264	0.416	1.99
61.0	116	.206	1.18
91.4	112	.227	1.45
152.4	90.0	.255	1.67

(d) $[90/0/90/0/45/0/-45/0]_s$

Crack length, 2a, mm	Strength, S_c, MPa	$\frac{S_{net}}{F_{tu}}$	Fracture toughness, K_Q, GPa-mm$^{1/2}$
W = 100 mm			
10.2	305	0.445	1.34
	299	.436	1.31
	269	.392	1.16
	321	.468	1.43
20.3	224	0.368	1.36
	224	.368	1.36
	223	.366	1.36
	244	.401	1.49
30.5	154	0.290	1.16
	169	.318	1.27
	192	.362	1.46
	216	.407	1.67
50.8	129	0.343	1.40
	132	.351	1.44
	125	.332	1.36
	119	.317	1.30
W = 305 mm			
30.5	190	0.276	1.36
61.0	133	.218	1.35
91.4	131	.245	1.70
152.4	83.7	.219	1.55

TABLE II.- Continued

(e) $[45/0/-45/0]_s$

Crack length, 2a, mm	Strength, S_c, MPa	$\frac{S_{net}}{F_{tu}}$	Fracture toughness, K_Q, GPa-mm$^{1/2}$
W = 100 mm			
10.2	316	0.467	1.40
	315	.466	1.40
	296	.438	1.30
	332	.491	1.50
20.3	222	0.370	1.35
	269	.448	1.68
	269	.448	1.68
	244	.407	1.50
30.5	228	0.436	1.77
	237	.453	1.85
	201	.384	1.54
	214	.409	1.65
50.8	131	0.354	1.43
	154	.416	1.70
	146	.394	1.61
	142	.383	1.56
W = 305 mm			
30.5	210	0.310	1.52
61.0	151	.251	1.55
91.4	177	.336	2.32
152.4	102	.271	1.90

(f) $[45/0/-45/0]_{2s}$

Crack length, 2a, mm	Strength, S_c, MPa	$\frac{S_{net}}{F_{tu}}$	Fracture toughness, K_Q, GPa-mm$^{1/2}$
W = 100 mm			
10.2	355	0.525	1.63
	305	.451	1.34
	321	.475	1.43
	314	.464	1.39
20.3	250	0.417	1.54
	257	.428	1.59
	236	.393	1.45
	249	.415	1.54
30.5	220	0.420	1.70
	211	.403	1.63
	234	.447	1.73
	195	.373	1.49
50.8	155	0.418	1.71
	155	.418	1.71
	142	.383	1.56
	151	.408	1.67
W = 305 mm			
30.5	264	0.390	1.96
61.0	151	.251	1.55
91.4	140	.266	1.81
152.4	99.3	.264	1.85

TABLE II.- Continued

(g) $[\pm 45/0/\pm 45/\bar{0}]_s$

Crack length, 2a, mm	Strength, S_c, MPa	$\frac{S_{net}}{F_{tu}}$	Fracture toughness, K_Q, GPa-mm$^{1/2}$	Remarks
W = 100 mm				
10.2	279	0.621	1.36	(a)
	268	.596	1.28	(a)
	279	.621	1.36	(a)
	274	.610	1.33	(a)
20.3	234	0.587	1.55	(a)
	235	.590	1.55	(a)
	217	.545	1.41	(a)
	221	.555	1.44	(b)
30.5	191	0.550	1.53	(a)
	177	.509	1.41	(a)
	190	.547	1.52	(a)
	179	.515	1.42	(b)
50.8	135	0.549	1.53	(a)
	140	.569	1.59	(a)
	138	.561	1.56	(a)
	129	.524	1.45	(a)
W = 305 mm				
30.5	221	0.491	1.72	(a)
61.0	171	.428	1.84	(b)
91.4	152	.434	2.03	(a)
152.4	109	.436	2.08	(a)

[a] $[45/-45/0/-45/45/0/45/-45/0/45/-45]_T$.
[b] $[45/-45/0/45/-45/0/-45/45/0/-45/45]_T$.

(h) $[45/0/-45/90]_s$

Crack length, 2a, mm	Strength, S_c, MPa	$\frac{S_{net}}{F_{tu}}$	Fracture toughness, K_Q, GPa-mm$^{1/2}$	Remarks
W = 100 mm				
10.2	280	0.607	1.35	(a)
	260	.563	1.22	(a)
	267	.578	1.26	(a)
	256	.555	1.19	(b)
20.3	210	0.513	1.34	(a)
	210	.513	1.34	(a)
	201	.491	1.27	(a)
	210	.513	1.34	(b)
30.5	173	0.484	1.36	(a)
	168	.470	1.32	(a)
	181	.507	1.43	(a)
	186	.521	1.48	(a)
50.8	120	0.475	1.34	(a)
	117	.463	1.30	(a)
	119	.471	1.32	(a)
	119	.471	1.33	(b)
W = 305 mm				
30.5	183	0.396	1.36	(a)
61.0	128	.311	1.32	(a)
91.4	118	.328	1.54	(a)
152.4	86.6	.337	1.63	(a)

[a] $[45/0/-45/90]_s$.
[b] $[45/90/-45/0]_s$.

TABLE II.- Concluded

(i) $[90/45/90/-45]_s$

Crack length, 2a, mm	Strength, S_c, MPa	$\frac{S_{net}}{F_{tu}}$	Fracture toughness, K_Q, GPa-mm$^{1/2}$
W = 100 mm			
10.2	164	1.041	
	170	1.080	(a)
	179	1.137	(a)
	155	.986	1.38
	160	1.018	
20.3	128	0.915	1.12
	143	1.021	
	124	.884	1.04
	131	.937	1.18
30.5	113	0.930	1.15
	100	.822	.93
	107	.873	1.02
	104	.851	.98
50.8	72.5	0.839	0.89
	72.2	.837	.89
	77.7	.900	.98
W = 305 mm			
30.5	122	0.775	1.20
61.0	102	.723	1.27
91.4	83.6	.681	1.23
152.4	53.5	.610	1.06

[a]Specimen failed away from slot.

(j) $[\pm 45]_{2s}$

Crack length, 2a, mm	Strength, S_c, MPa	$\frac{S_{net}}{F_{tu}}$	Fracture toughness, K_Q, GPa-mm$^{1/2}$
W = 100 mm			
10.2	138	0.962	1.12
	143	1.002	
	138	.964	1.13
	136	.951	1.08
20.3	123	0.969	1.17
	125	.981	1.21
	121	.951	1.12
	119	.939	1.08
30.5	110	0.990	1.18
	106	.956	1.10
	107	.961	1.11
	106	.952	1.09
50.8	73.2	0.933	0.94
	75.7	.965	.98
	74.7	.952	.97
	74.0	.943	.95
W = 305 mm			
30.5	131	0.912	1.62
61.0	115	.903	1.72
91.4	102	.910	1.75
152.4	69.1	.867	1.48

TABLE III.- FRACTURE DATA FOR T300/BP-907 LAY-UPS

(a) $[45/0/-45/0]_{2s}$

Crack length, 2a, mm	Strength, S_c, MPa	$\frac{S_{net}}{F_{tu}}$	Fracture toughness, K_Q, GPa-mm$^{1/2}$
W = 50 mm			
5.0	345	0.605	1.16
	342	.599	1.15
	343	.601	1.15
	338	.592	1.13
10.0	270	0.532	1.22
	296	.584	1.37
	276	.544	1.25
	266	.524	1.20
20.0	183	0.481	1.21
	186	.489	1.22
	194	.510	1.29
	184	.484	1.21
W = 100 mm			
20.0	226	0.446	1.40
	214	.422	1.31
	201	.396	1.22
	198	.390	1.20
40.0	130	0.342	1.18
	123	.323	1.11
	141	.371	1.28
	131	.344	1.18

TABLE III.- Continued

(b) $[45/0/-45/90]_{2s}$

Crack length, 2a, mm	Strength, S_c, MPa	$\frac{S_{net}}{F_{tu}}$	Fracture toughness, K_Q, GPa-mm$^{1/2}$	Remarks
W = 50 mm				
5.0	276	0.712	1.02	(a)
	287	.740	1.09	(a)
	287	.740	1.09	(a)
	286	.737	1.08	(a)
	278	.717	1.03	(b)
	276	.712	1.02	(b)
	294	.758	1.14	(b)
	278	.717	1.03	(b)
10.0	227	0.658	1.10	(a)
	226	.655	1.09	(a)
	223	.647	1.07	(a)
	226	.655	1.09	(a)
20.0	143	0.553	0.96	(a)
	132	.510	.87	(a)
	154	.596	1.05	(a)
	159	.615	1.09	(a)
	158	.611	1.08	(b)
	151	.584	1.02	(b)
	154	.596	1.05	(b)
	153	.592	1.04	(b)
W = 100 mm				
20.0	172	0.499	1.08	(a)
	156	.452	.96	(a)
	172	.499	1.08	(a)
	173	.502	1.09	(a)
40.0	114	0.441	1.05	(a)
	102	.394	.93	(a)
	115	.445	1.06	(a)
	109	.422	1.01	(a)

[a] $[45/0/-45/90]_{2s}$.
[b] $[45/90/-45/0]_{2s}$.

TABLE III.- Concluded

(c) $[\pm 45]_{2s}$

Crack length, 2a, mm	Strength, S_c, MPa	$\frac{S_{net}}{F_{tu}}$	Fracture toughness, K_Q, GPa-mm$^{1/2}$	Failing strain, ε_{oc}	$K_{Q\varepsilon}$, mm$^{1/2}$
W = 50 mm					
5.0	198	1.11		0.101	
	180	1.01		.0807	
	203	1.14		.108	
	198	1.11		.102	
	203	1.14		.107	
20.0	89.4	0.752	0.65	0.00881	0.0552
	88.8	.747	.65	.00861	.0540
	90.7	.763	.67	.00923	.0579
	84.0	.707	.60	.00759	.0475
	89.7	.755	.66	.00885	.0555

TABLE IV.- MEASURED AND PREDICTED VALUES OF K_Q

Lay-up	Predicted K_Q, GPa-$\sqrt{mm}$	Average measured K_Q, GPa-$\sqrt{mm}$	Coefficient of variation
T300/5208			
$[0]_{8T}$	2.126		
$[0_2/90/0]_s$	1.590	5.600	0.283
$[0_2/45/0_2/-45/0_2]_s$	2.000	3.260	.194
$[90/0]_{2s}$	1.110	1.430	.180
$[90/0/90/0/45/0/-45/0]_s$	1.380	1.390	.0993
$[45/0/-45/0]_s$	1.770	1.610	.144
$[45/0/-45/0]_{2s}$	1.770	1.610	.0981
$[\pm45/0/\pm45/\bar{0}]_s$	1.50	1.550	.141
$[45/0/-45/90]_s$	1.110	1.350	.0753
$[90/45/90/-45]_s$	.704	1.090	.139
$[\pm45]_{2s}$	1.110	1.200	.210
T300/BP-907			
$[0]_{8T}$	1.791		
$[45/0/-45/0]_{2s}$	1.480	1.220	0.0623
$[45/0/-45/90]_{2s}$	.928	1.050	.0557
$[\pm45]_{2s}$	.928	.644	.0394

TABLE V.- PREDICTED SPLIT LENGTHS

Laminate	0° plies (α = 0°)				±45° plies (α = 45°)				90° plies (α = 90°) (a)		
	$\ell_{1\alpha'}$ mm	$\ell_{2\alpha'}$ mm	$\ell_{12\alpha'}$ mm	$\ell_{\alpha'}$ mm	$\ell_{1\alpha'}$ mm	$\ell_{2\alpha'}$ mm	$\ell_{12\alpha'}$ mm	$\ell_{\alpha'}$ mm	$\ell_{1\alpha'}$ mm	$\ell_{2\alpha'}$ mm	$\ell_{\alpha'}$ mm
T300/5208											
$[0]_{8T}$	0.46	7.83	6.17	13.20							
$[0_2/90/0]_s$	.36	2.51	4.46	6.69					0.34	2.91	2.25
$[0_2/45/0_2/-45/0_2]_s$	.37	2.20	1.51	3.48	0.58	2.98	0.00	2.24			
$[90/0]_{2s}$	.41	.63	2.64	3.18					.14	2.24	1.82
$[90/0/90/0/45/0/-45/0]_s$	.28	.57	.92	1.37	.26	1.33	.12	1.12	.23	2.55	2.01
$[45/0/-45/0]_s$	.35	.29	.62	.95	.39	2.24	.08	1.78			
$[45/0/-45/0]_{2s}$	.35	.29	.62	.95	.39	2.24	.08	1.78			
$[\pm45/0/\pm45/\bar{0}]_s$	.37	.06	.32	.60	.29	1.85	.38	1.78			
$[45/0/-45/90]_s$	.25	.29	.32	.58	.19	1.40	.27	1.34	.14	2.23	1.81
$[90/45/90/-45]_s$					.19	2.19	.71	2.44	.08	2.97	2.57
$[\pm45]_{2s}$					.25	1.90	2.13	3.58			
T300/BP-907											
$[0]_{8T}$	0.19	2.74	3.04	5.54							
$[45/0/-45/0]_{2s}$	.14	.07	.31	.43	0.16	0.54	0.04	0.44			
$[45/0/-45/90]_{2s}$	.10	.07	.16	.25	.08	.34	.14	.39	0.06	0.53	0.42
$[\pm45]_{2s}$					.10	.45	1.05	1.39			

[a]For α = 90°, $\ell_{12\alpha}$ = 0.

TABLE VI.- PREDICTED ELASTIC CONSTANTS AND K_Q VALUES FOR LAY-UPS OF T300 GRAPHITE, KEVLAR 49, AND S-GLASS AND FOR HYBRIDS

Lay-up	$E_{y'}$ GPa	$E_{x'}$ GPa	ν_{yx}	$G_{xy'}$ GPa	ξ	$K_{Q'}$ GPa-mm$^{1/2}$
T300 graphite/epoxy						
$[0/\pm45/90/0]_s$	51.4	51.4	0.307	19.7	0.694	1.11
$[0_2/\pm45/90]_s$	67.0	44.6	.307	16.9	.750	1.34
Kevlar 49/epoxy						
$[0/\pm45/90]_s$	28.1	28.1	0.336	10.5	0.664	1.05
$[0_2/\pm45/90]_s$	37.3	24.4	.339	8.83	.726	1.28
S-glass/epoxy						
$[0/\pm45/90]_s$	25.9	25.9	0.353	9.56	0.647	1.63
$[0_2/\pm45/90]_s$	30.6	24.7	.345	8.55	.691	1.80
Kevlar 49/T300 graphite/epoxy hybrid						
[a]$[0/\pm45/90]_s$	37.5	48.3	0.310	18.7	0.649	1.43
[a]$[0_2/\pm45/90]_s$	44.9	41.1	.312	15.4	.701	1.59
S-glass/T300-graphite/epoxy hybrid						
[a]$[0/\pm45/90]_s$	31.3	49.8	0.306	19.3	0.615	2.07
[a]$[0_2/\pm45/90]_s$	35.0	44.5	.305	16.3	.656	2.17

[a]Off-axis plies are T300 graphite/epoxy.

TABLE VII.- ALLOWABLE MATRIX STRESSES

5208	BP-907	Test method
σ_{1mu}, MPa		
57.6	90.0	Neat-resin tensile test
σ_{2u}, MPa		
		Tensile tests of lay-ups with -
38.3	52.9	All 90° plies
38.3	52.9	Four interior 90° plies[a]
38.3	52.9	Two surface 90° plies[a]
57.6	90.0	One surface 90° ply
57.6	90.0	Two interior 90° plies[a]
57.6	90.0	One interior 90° ply
τ_{12u}, MPa		
80.0	95.5	Tensile test of $[\pm 45]_{2s}$

[a]Contiguous plies.

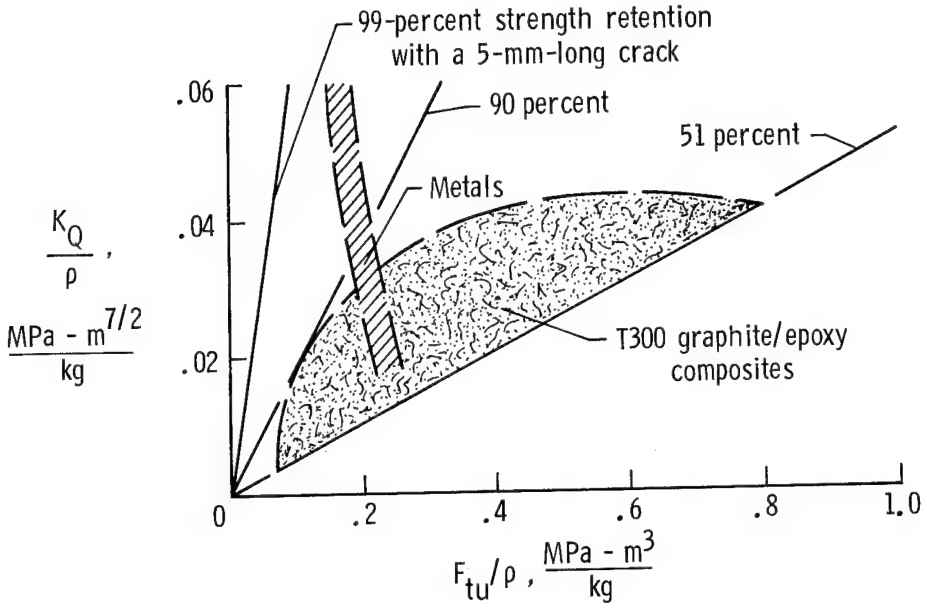

Figure 1.- Fracture toughness plotted against ultimate tensile strength for T300 graphite/epoxy composites and metals.

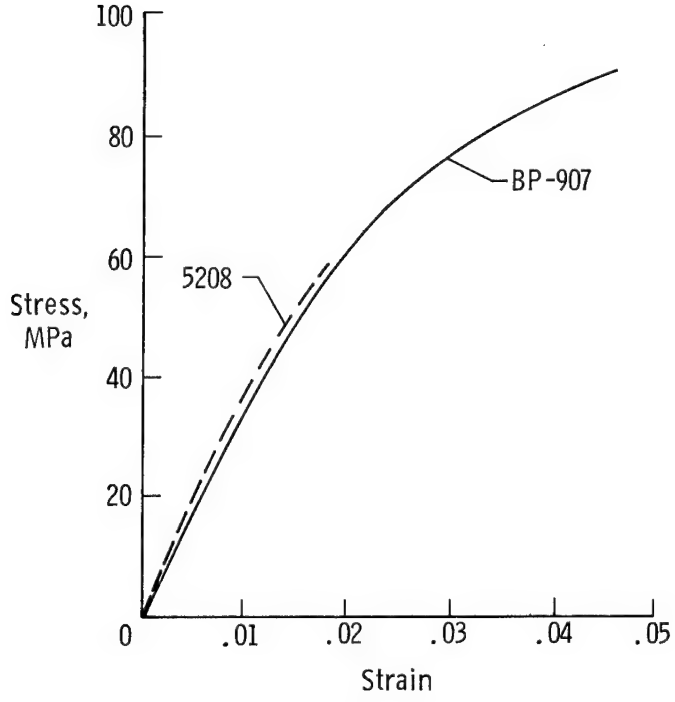

Figure 2.- Tensile stress-strain curves for 5208 and BP-907 neat resins.

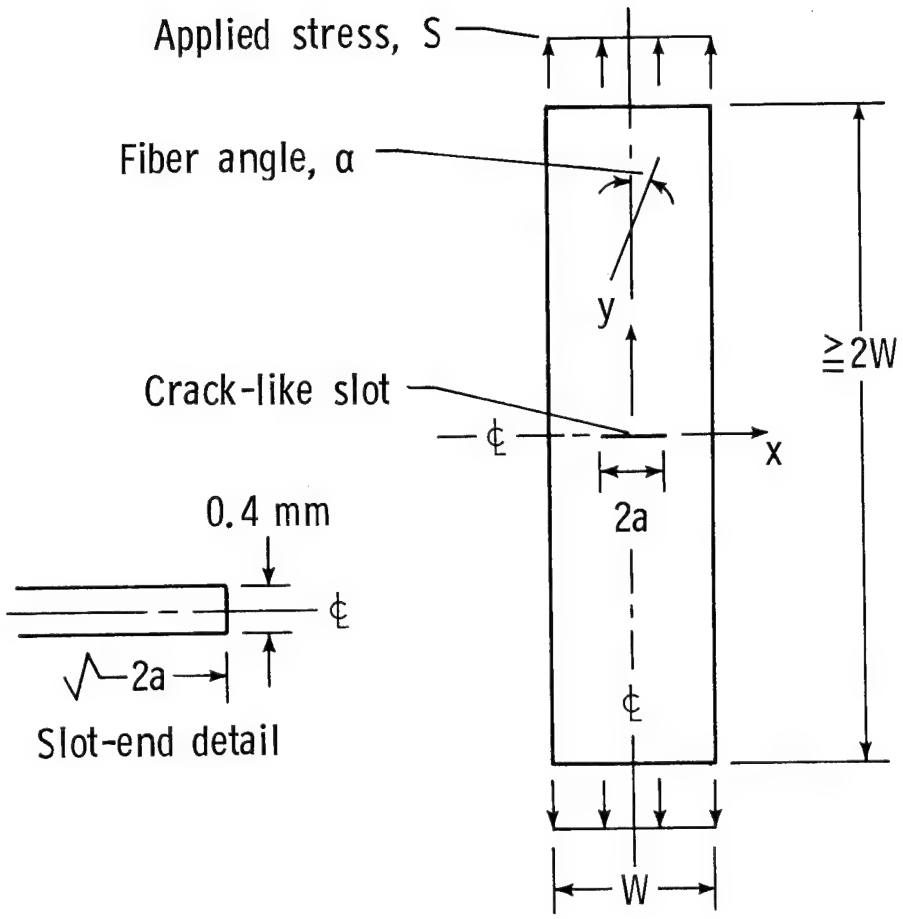

Figure 3.- Specimen configuration.

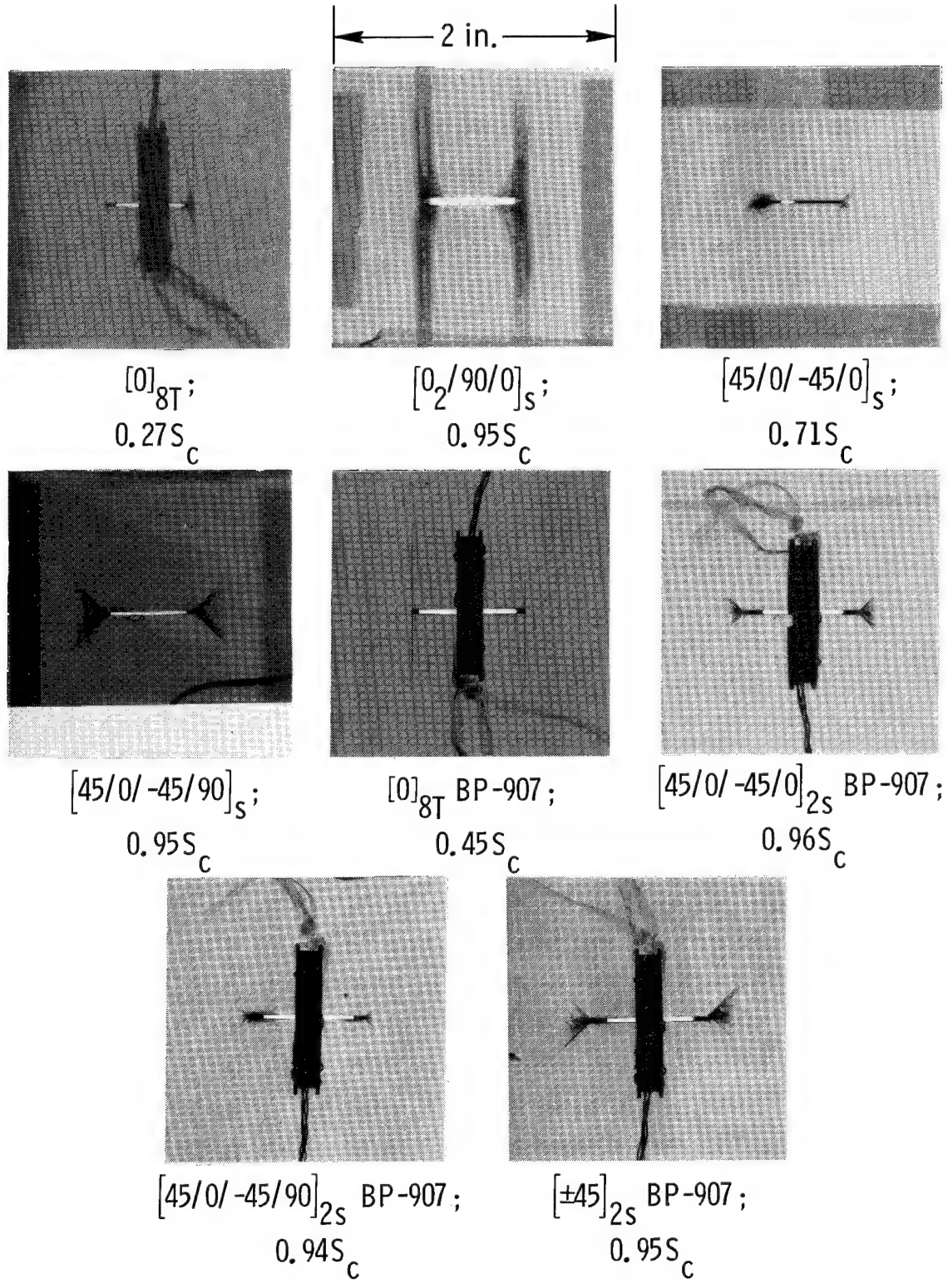

Figure 4.- Radiographs of 50-mm-wide specimens near failure. Applied stresses are given as a ratio to the failing stress. For 5208 specimens, 2a = 15 mm; for BP-907 specimens, 2a = 20 mm. Specimens are 5208 unless noted otherwise.

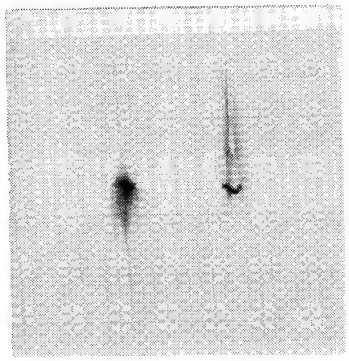

$[0_2/45/0_2/-45/0_2]_s$;
$0.95S_c$

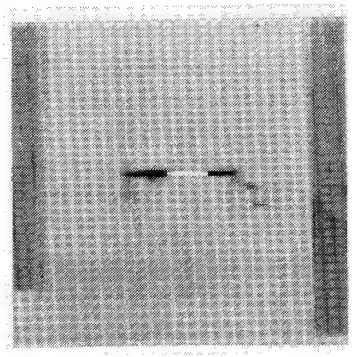

$[90/0]_{2s}$;
$0.91S_c$

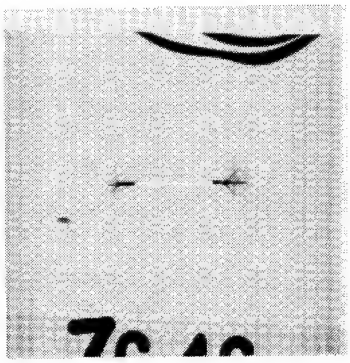

$[90/0/90/0/45/0/-45/0]_s$;
$0.99S_c$

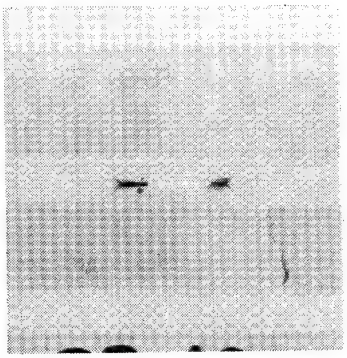

$[45/0/-45/0]_{2s}$;
$0.80S_c$

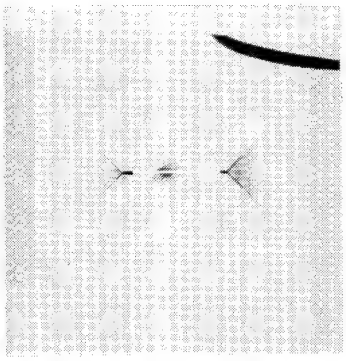

$[\pm45/0/\pm45/\bar{0}]_s$;
$0.95S_c$

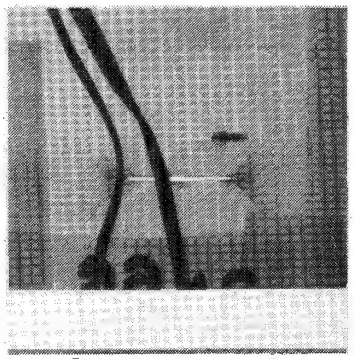

$[90/45/90/-45]_s$;
$0.98S_c$

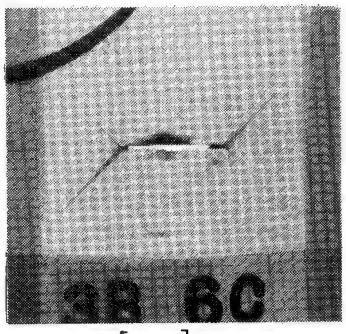

$[\pm45]_{2s}$;
$0.93S_c$

L-84-122

Figure 4.- Concluded.

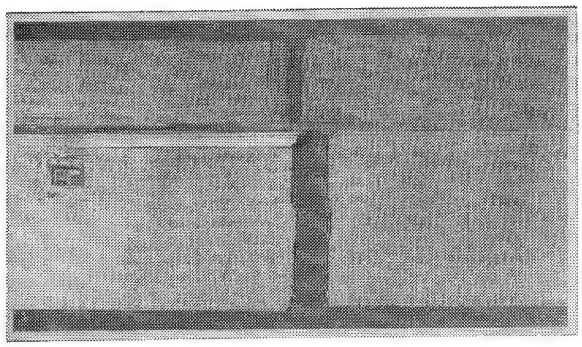

$[0_2/90/0]_s$

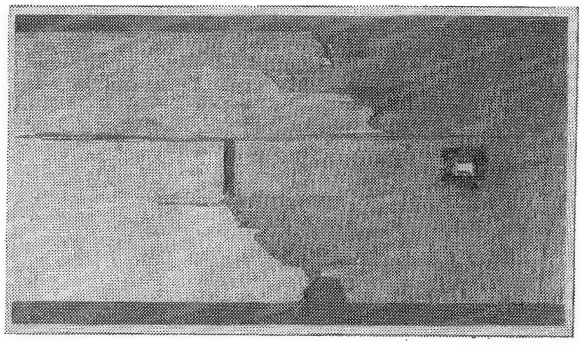

$[0_2/45/0_2/-45/0_2]_s$

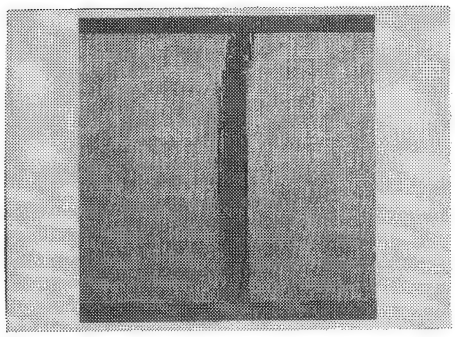

$[90/0]_{2s}$

Applied stress, S

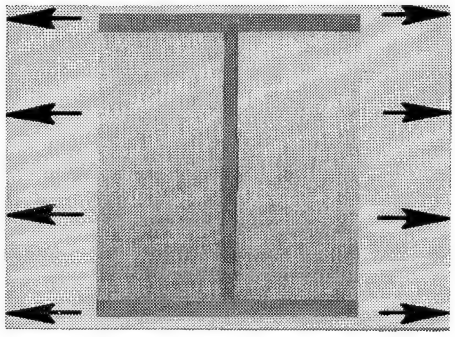

$[90/0/90/0/45/0/-45/0]_s$

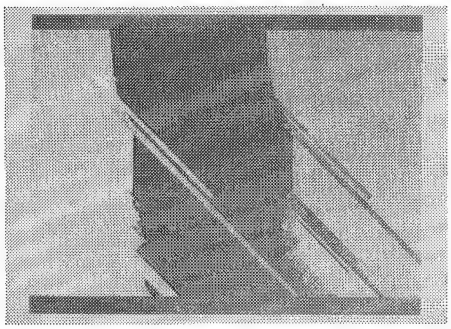

$[45/0/-45/0]_s$

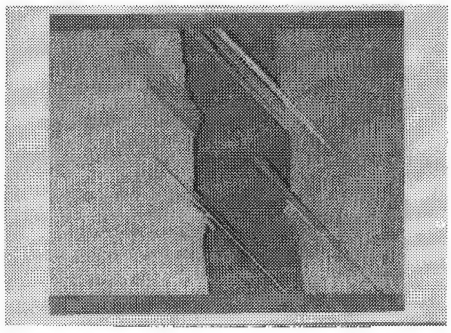

$[45/0/-45/0]_{2s}$

L-84-123

Figure 5.- Photographs of failed specimens.

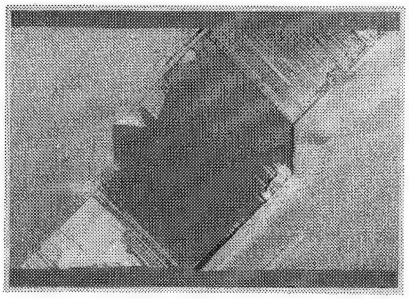

$[\pm 45/0/\pm 45/\bar{0}]_s$

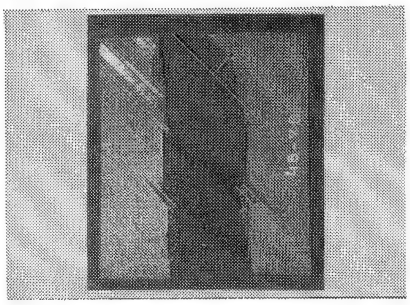

$[45/0/-45/90]_s$

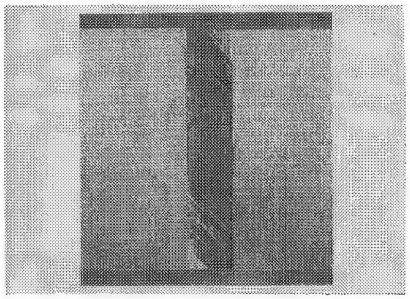

$[90/45/90/-45]_s$

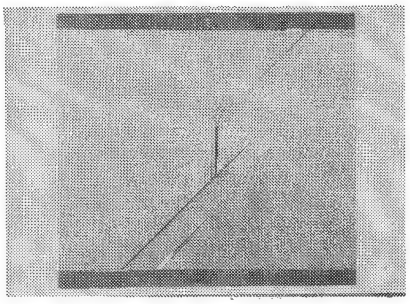

$[\pm 45]_{2s}$

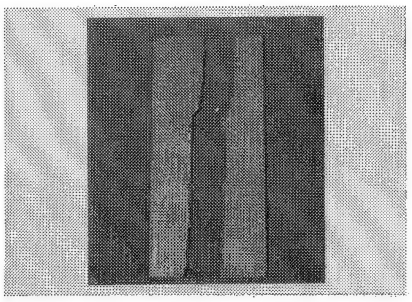

$[45/0/-45/0]_{2s}$ BP-907

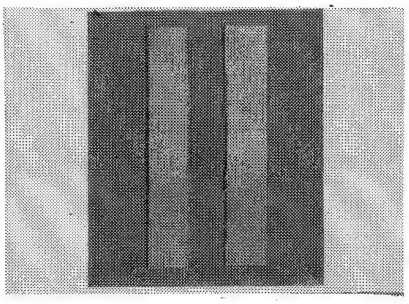

$[45/0/-45/90]_{2s}$ BP-907

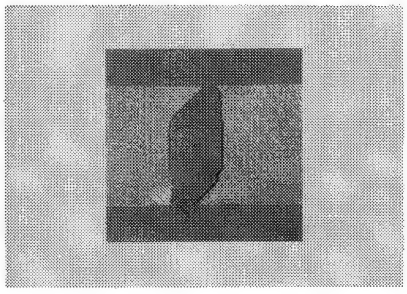

$[\pm 45]_{2s}$ BP-907

L-84-124

Figure 5.- Concluded.

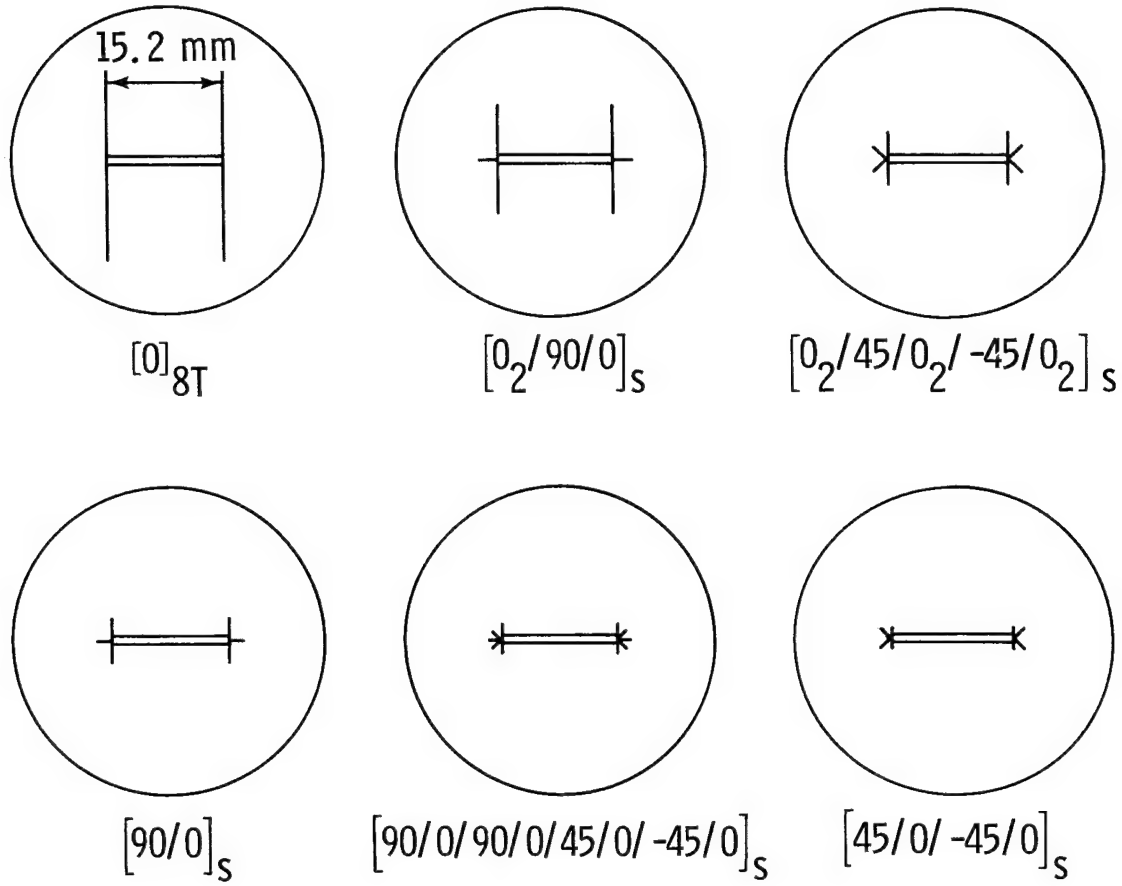

Figure 6.- Predicted splitting.

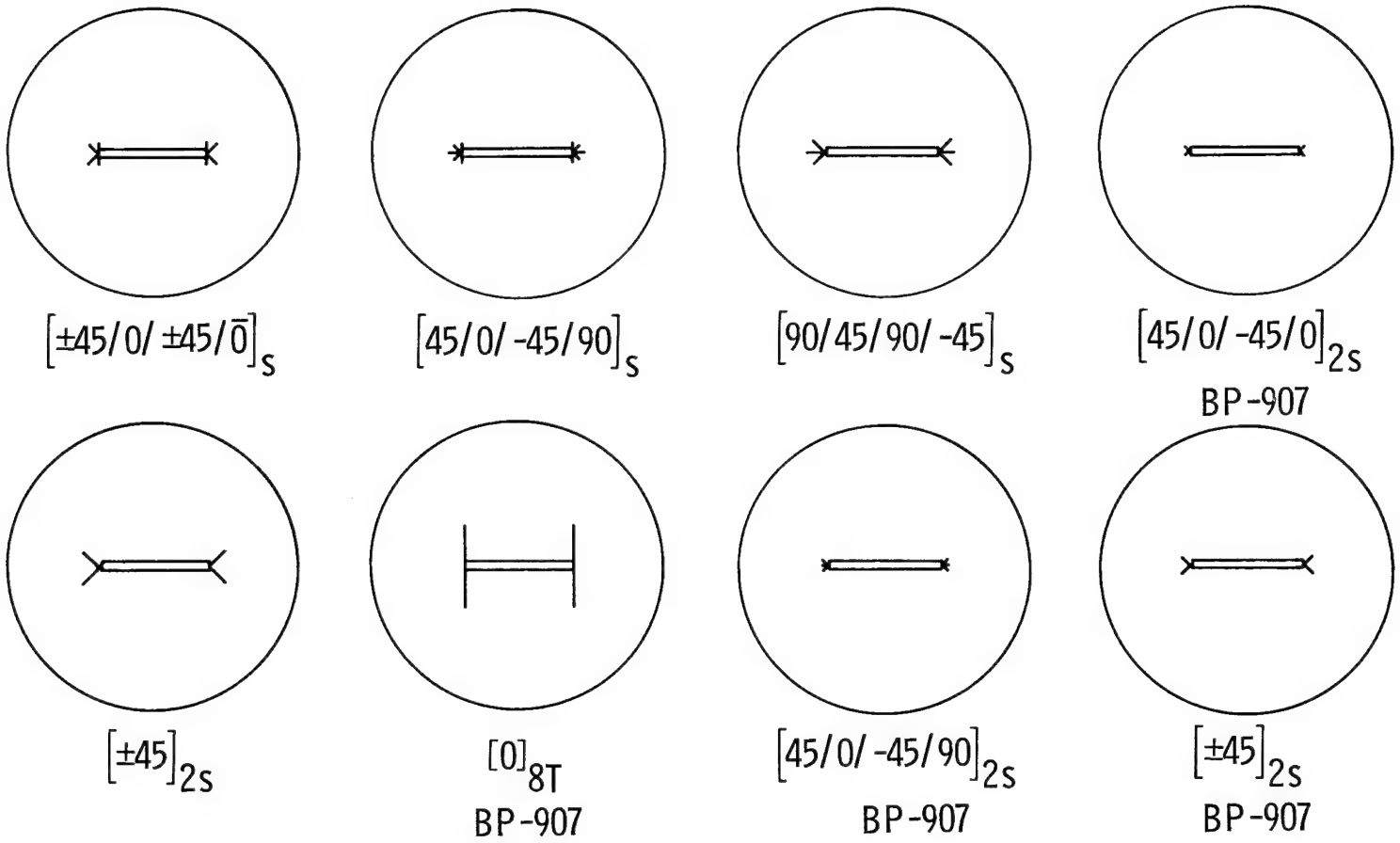

Figure 6.- Concluded.

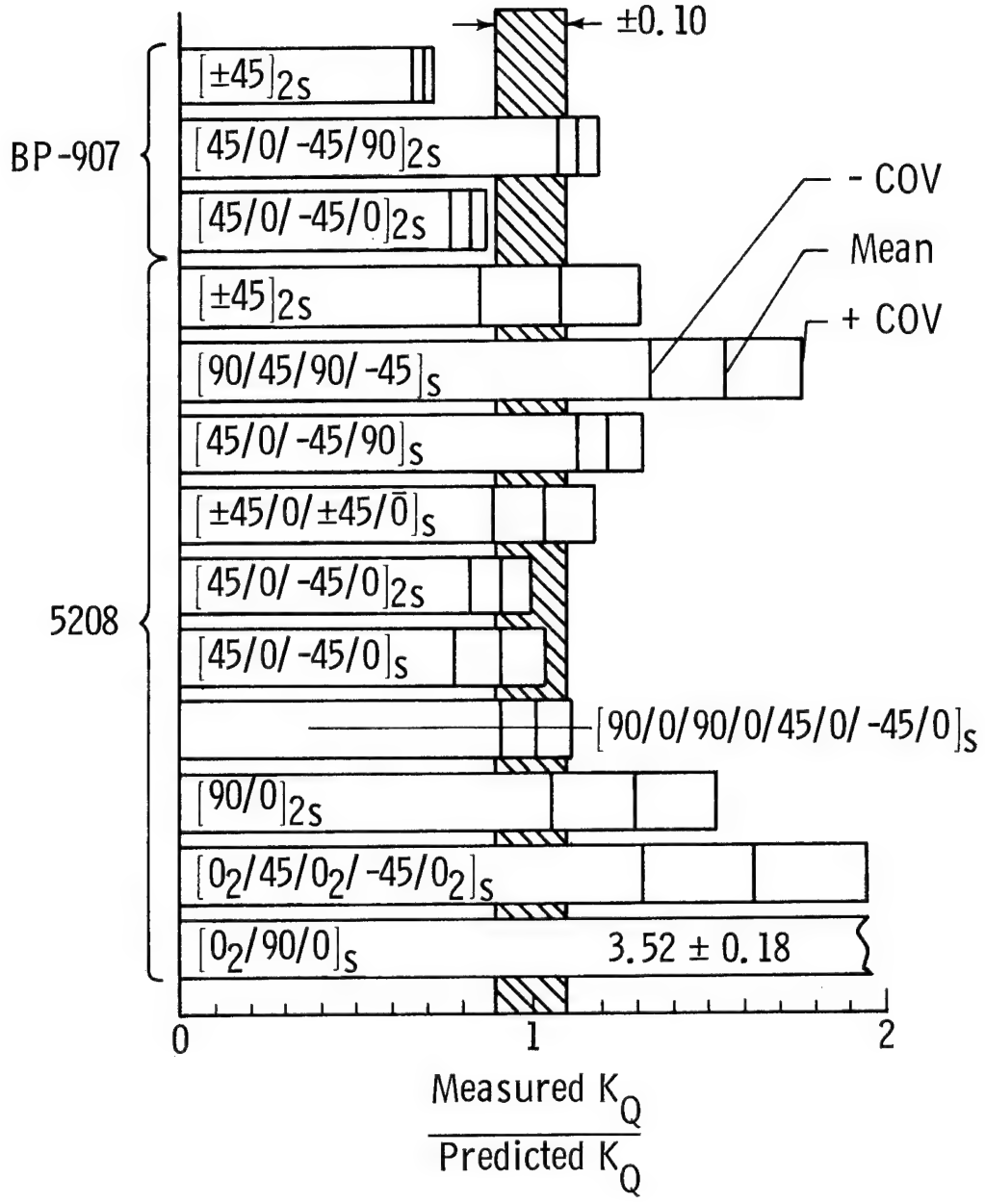

Figure 7.- Ratio of measured to predicted K_Q values.

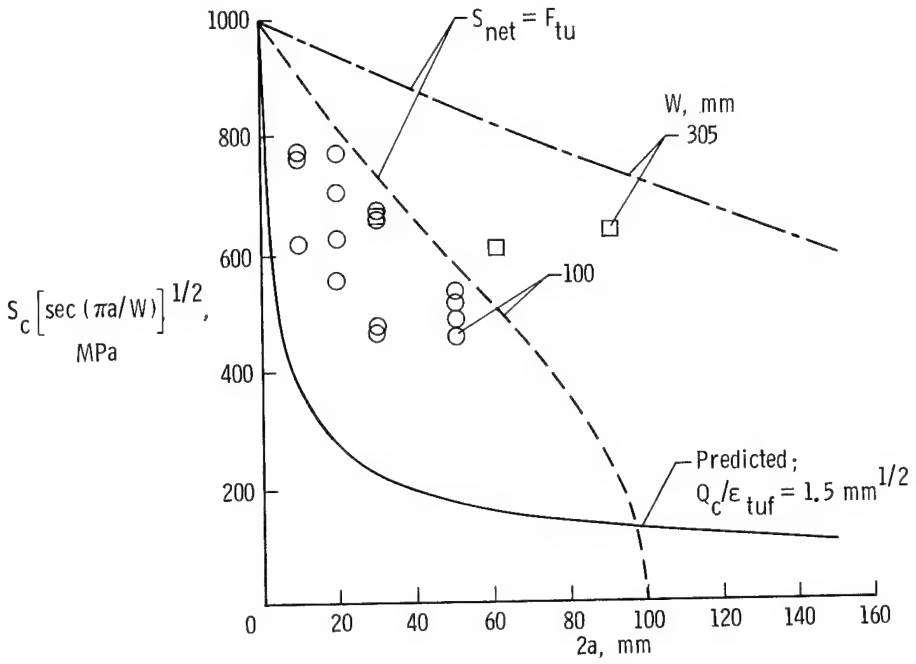

(a) $[0_2/90/0]_s$ T300/5208.

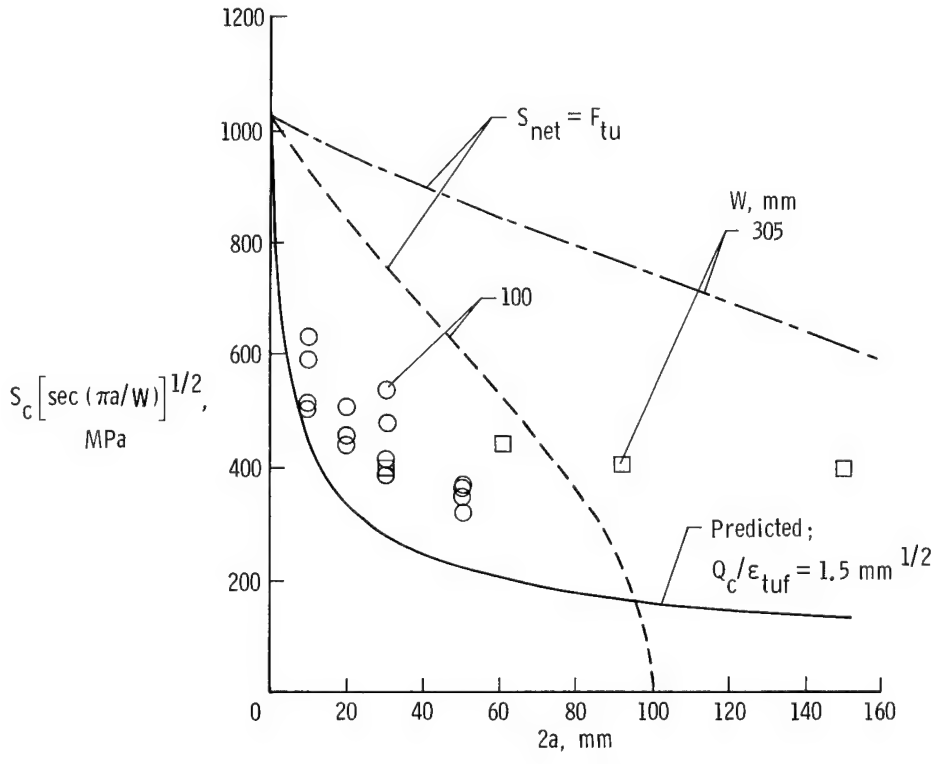

(b) $[0_2/45/0_2/-45/0_2]_s$ T300/5208.

Figure 8.- Measured and predicted strengths for lay-ups with 0° plies.

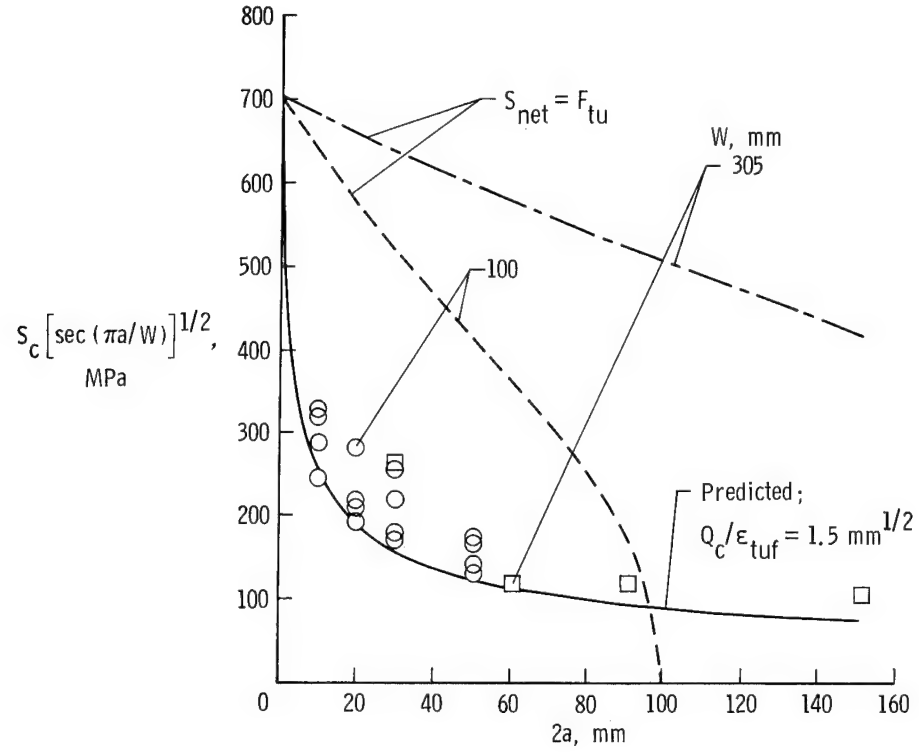

(c) $[90/0]_{2s}$ T300/5208.

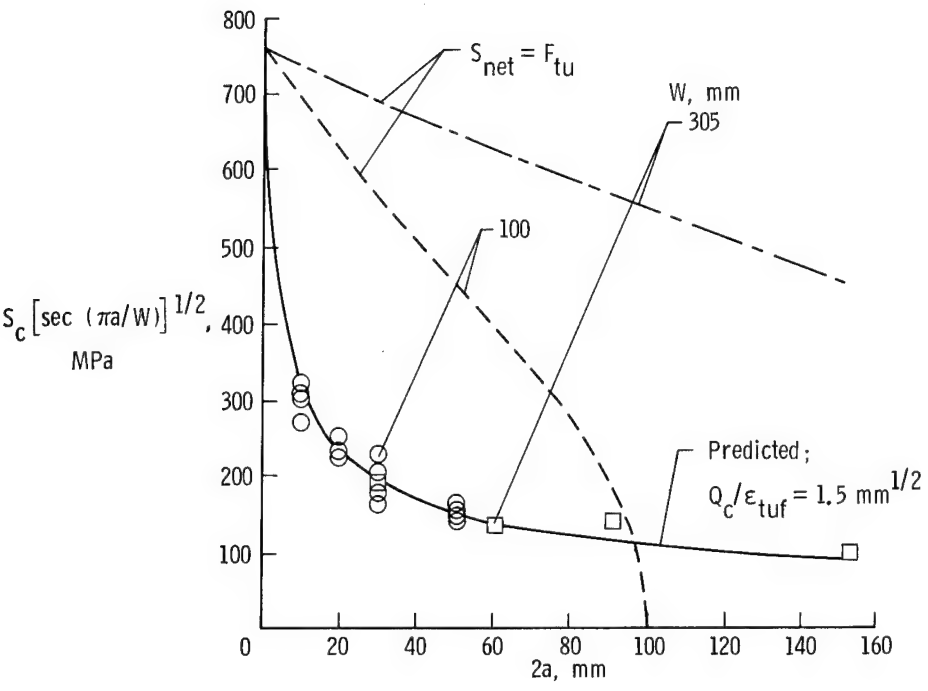

(d) $[90/0/90/0/45/0/-45/0]_s$ T300/5208.

Figure 8.- Continued.

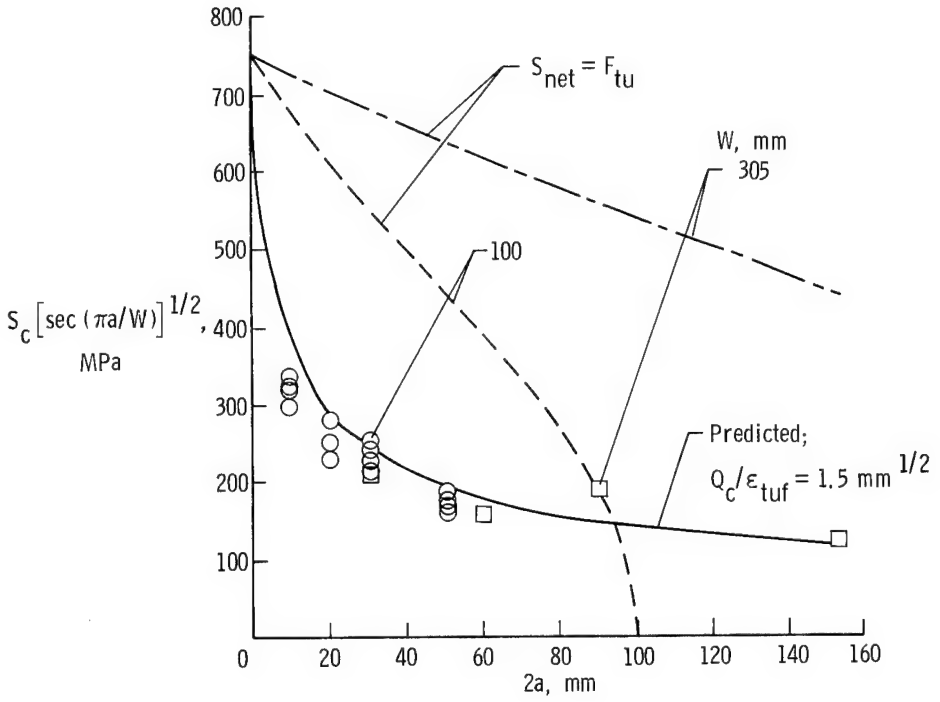

(e) $[45/0/-45/0]_s$ T300/5208.

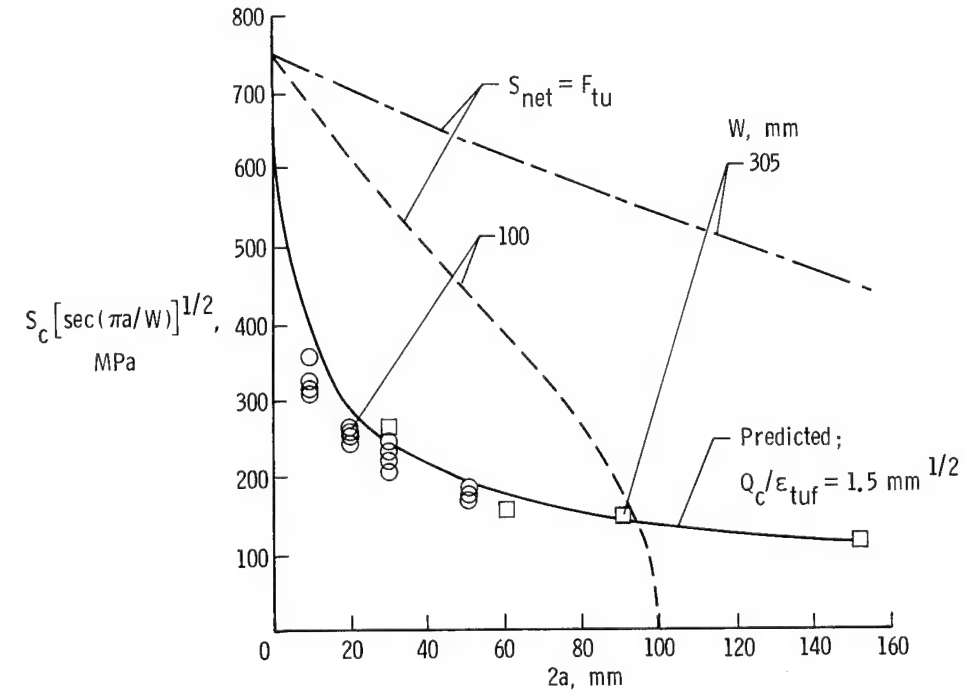

(f) $[45/0/-45/0]_{2s}$ T300/5208.

Figure 8.- Continued.

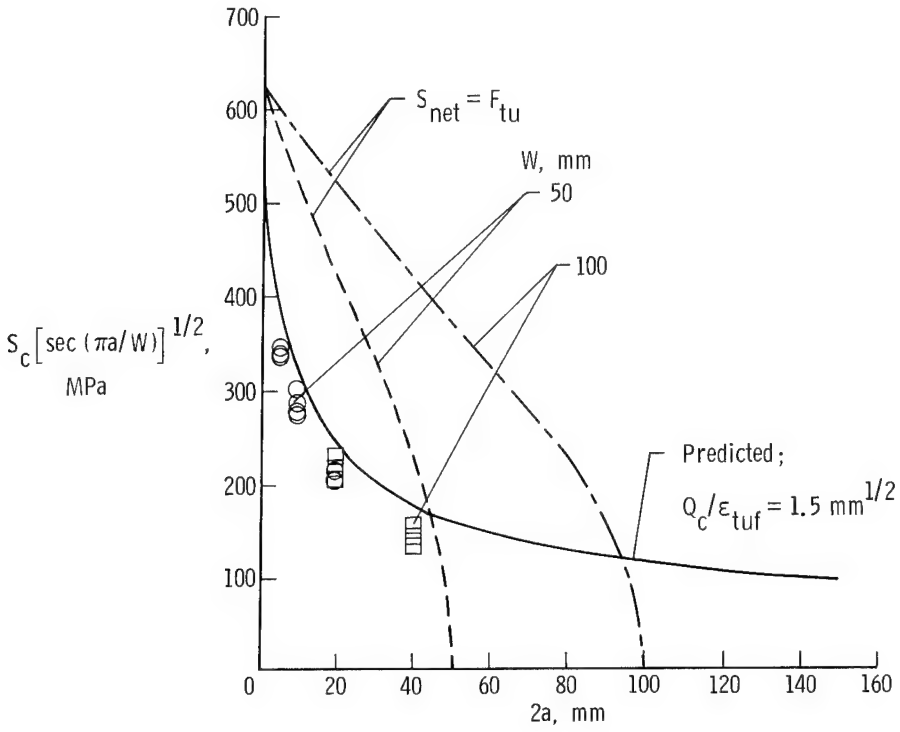

(g) $[45/0/-45/0]_{2s}$ T300/BP-907.

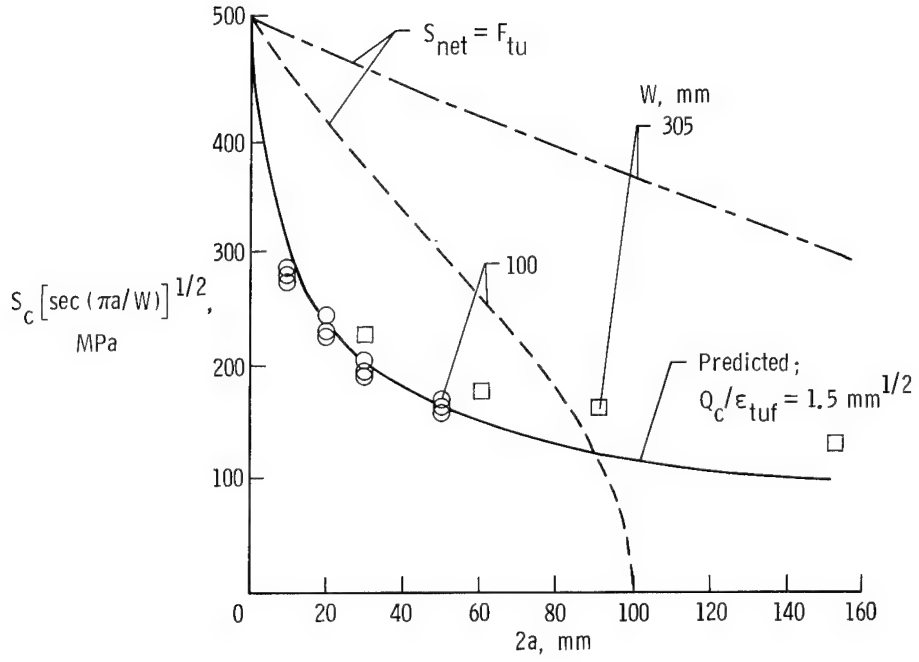

(h) $[\pm 45/0/\pm 45/\bar{0}]_s$ T300/5208.

Figure 8.- Continued.

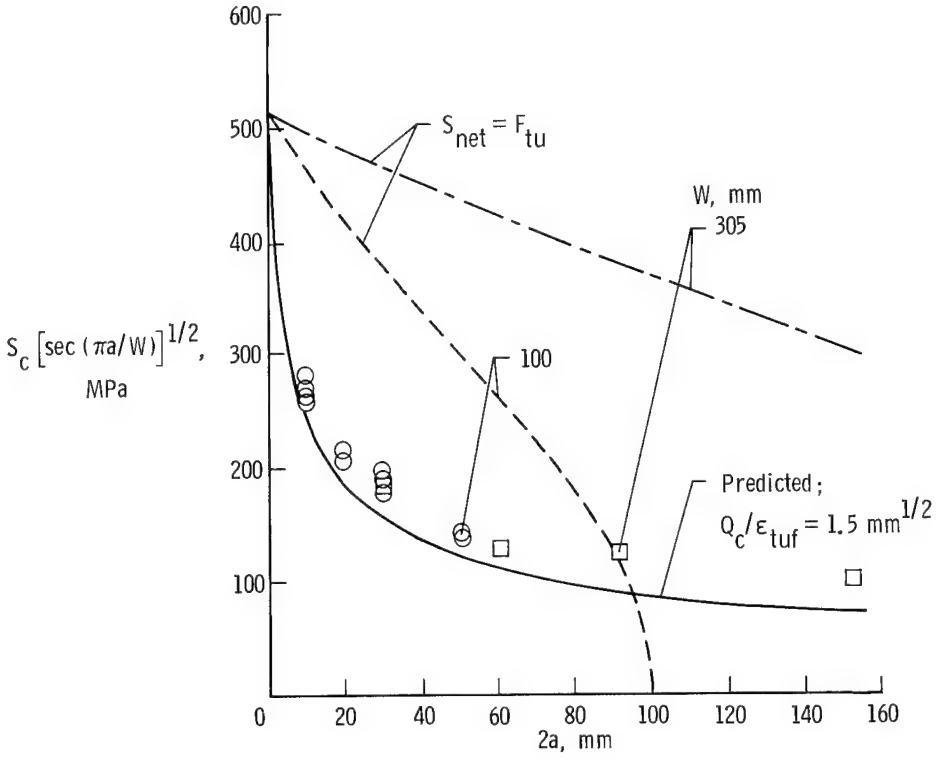

(i) $[45/0/-45/90]_s$ T300/5208.

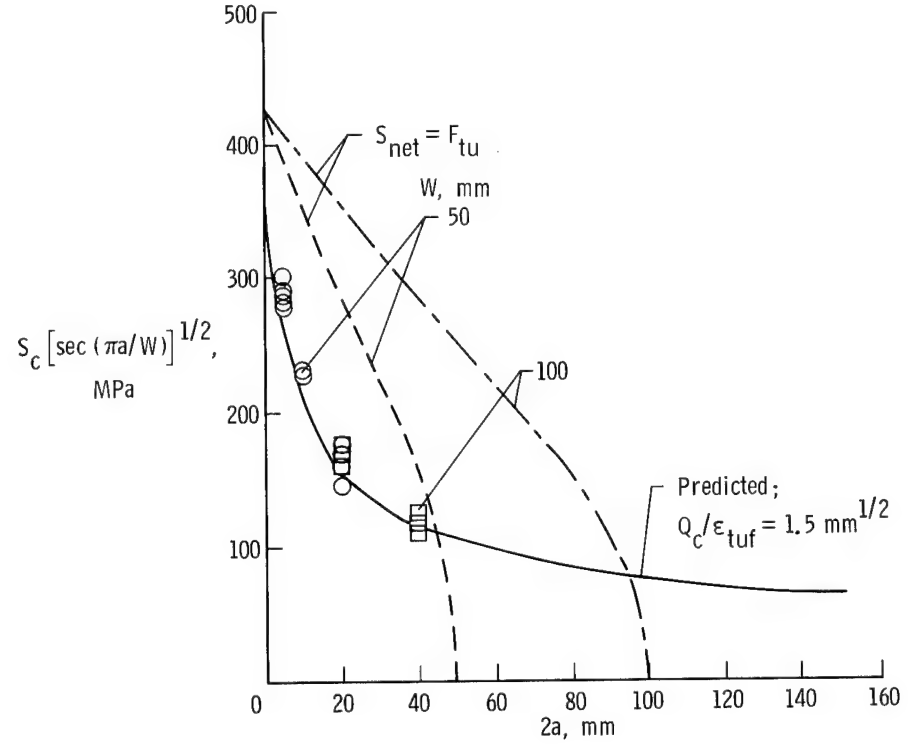

(j) $[45/0/-45/90]_{2s}$ T300/BP-907.

Figure 8.- Concluded.

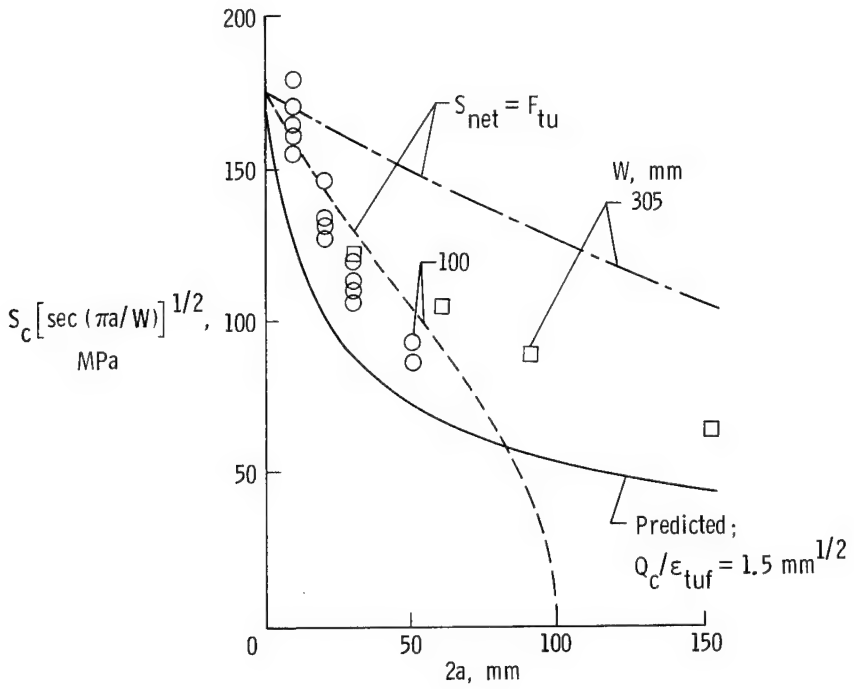

(a) $[90/45/90/-45]_s$ T300/5208.

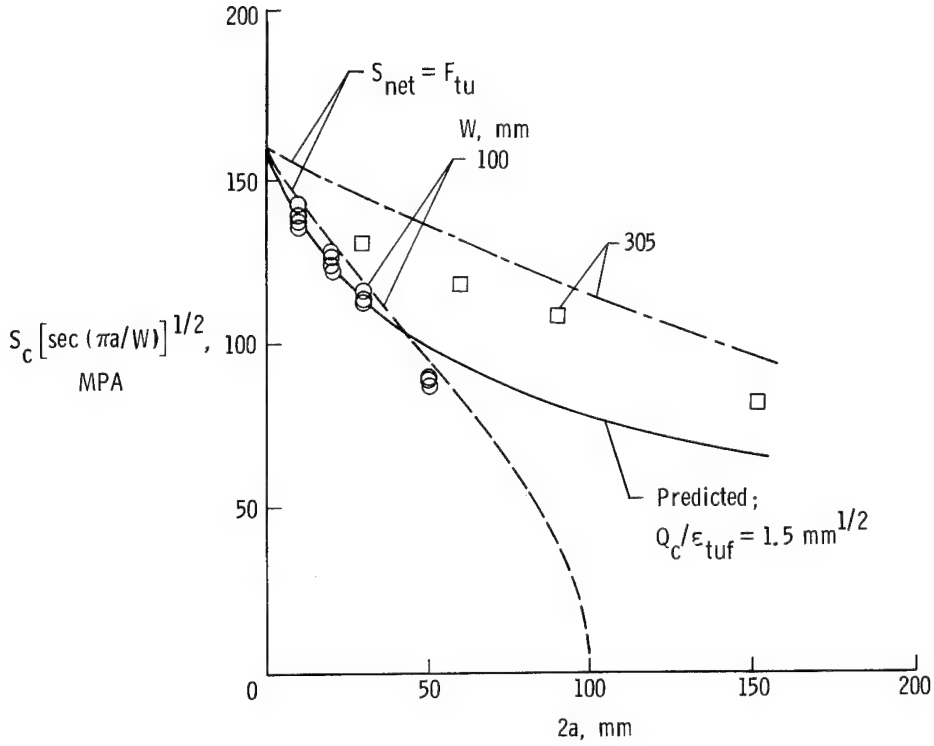

(b) $[\pm 45]_{2s}$ T300/5208.

Figure 9.- Measured and predicted strengths for lay-ups without 0° plies.

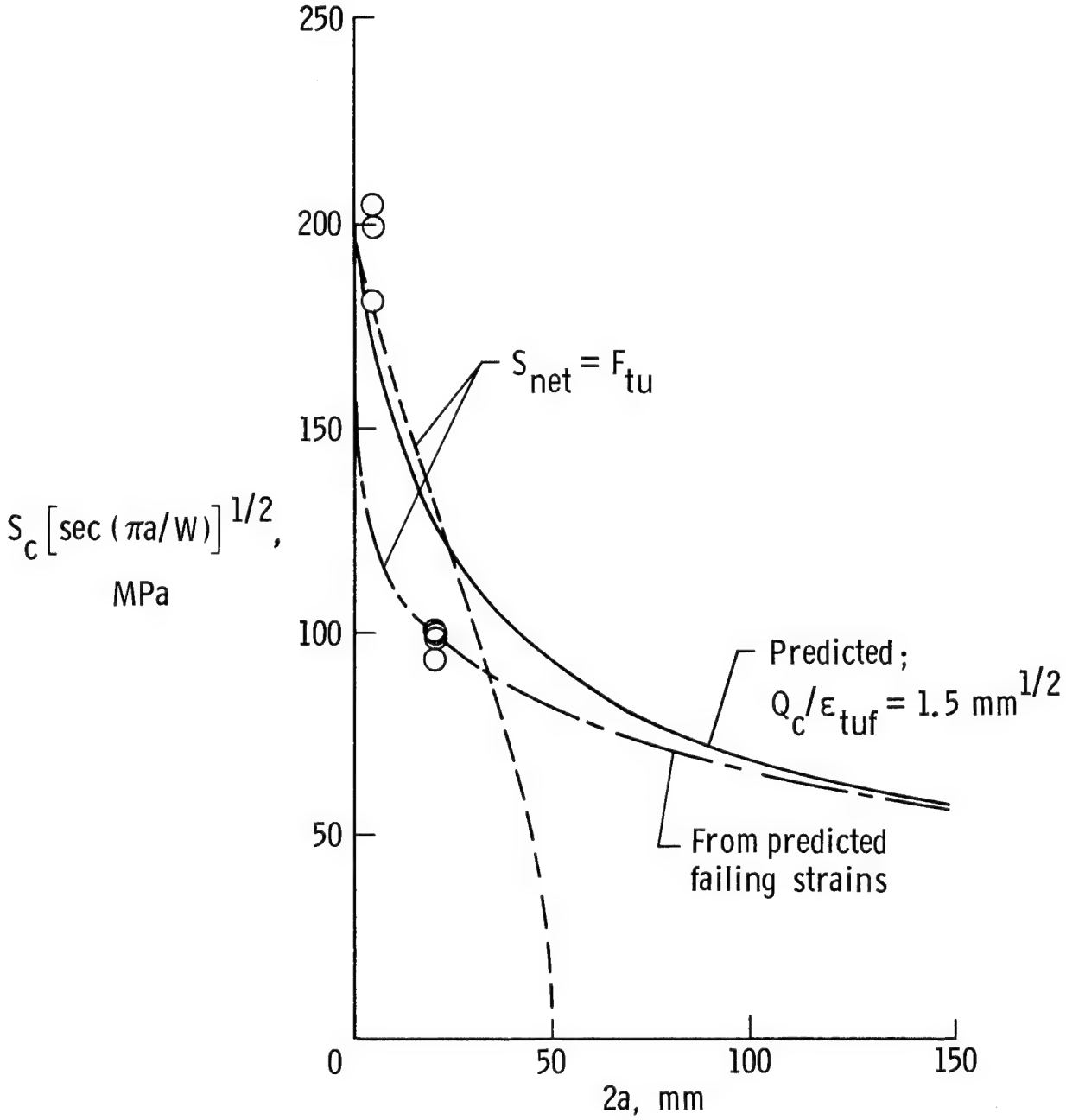

(c) $[\pm 45]_{2s}$ T300/BP-907; W = 50 mm.

Figure 9.- Concluded.

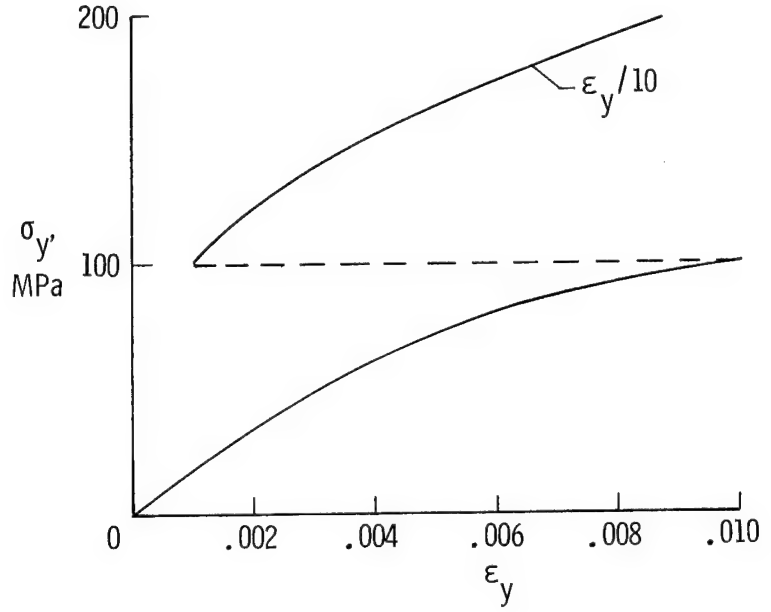

Figure 10.- Tension stress-strain curve for $[\pm 45]_{2s}$ BP-907.

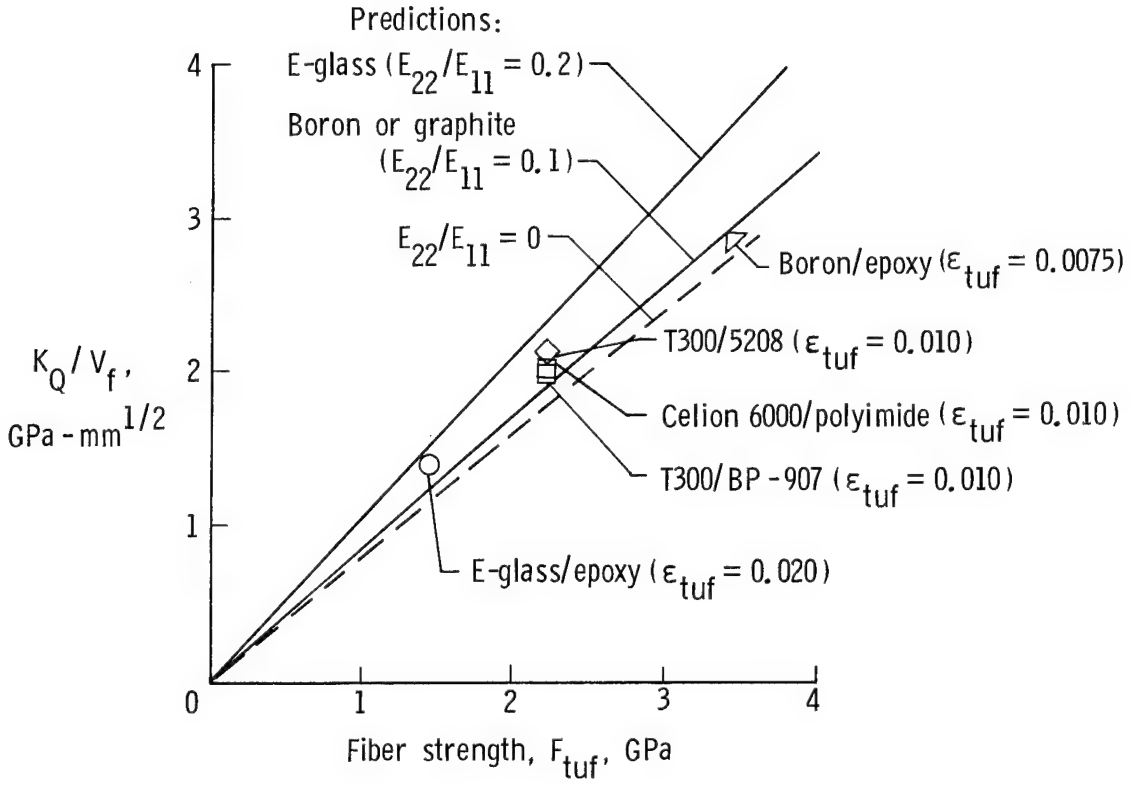

Figure 11.- Effect of fiber strength on K_Q of $[0/\pm 45/90]_s$ laminates.

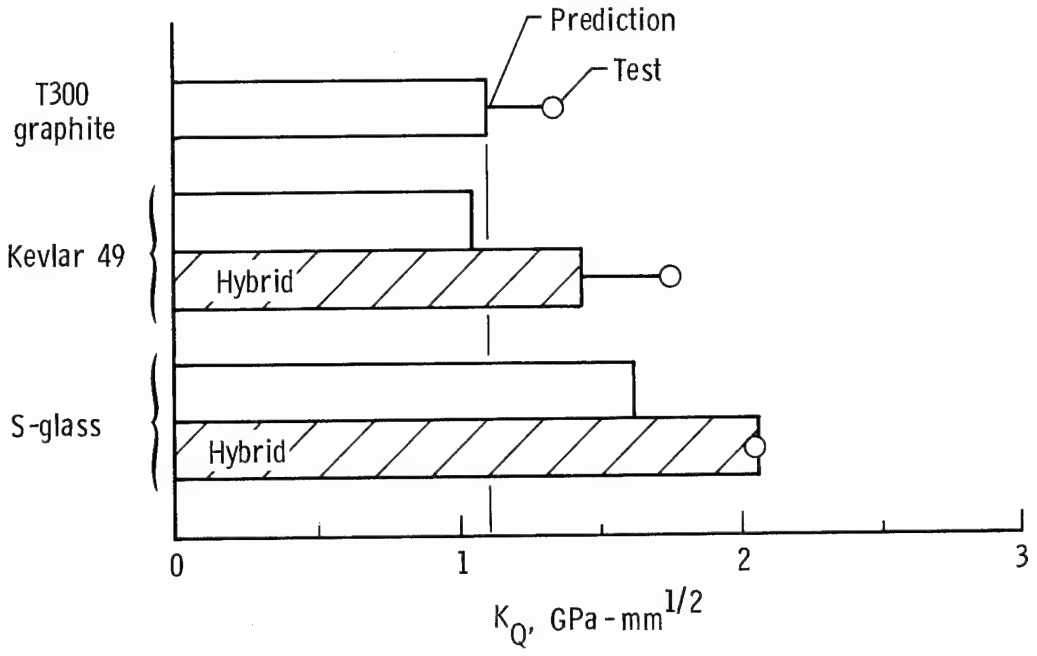

Figure 12.- Values of K_Q for $[45/0/-45/90]_{2s}$ hybrids with 5208 matrix. For hybrids, off-axis plies are T300 graphite.

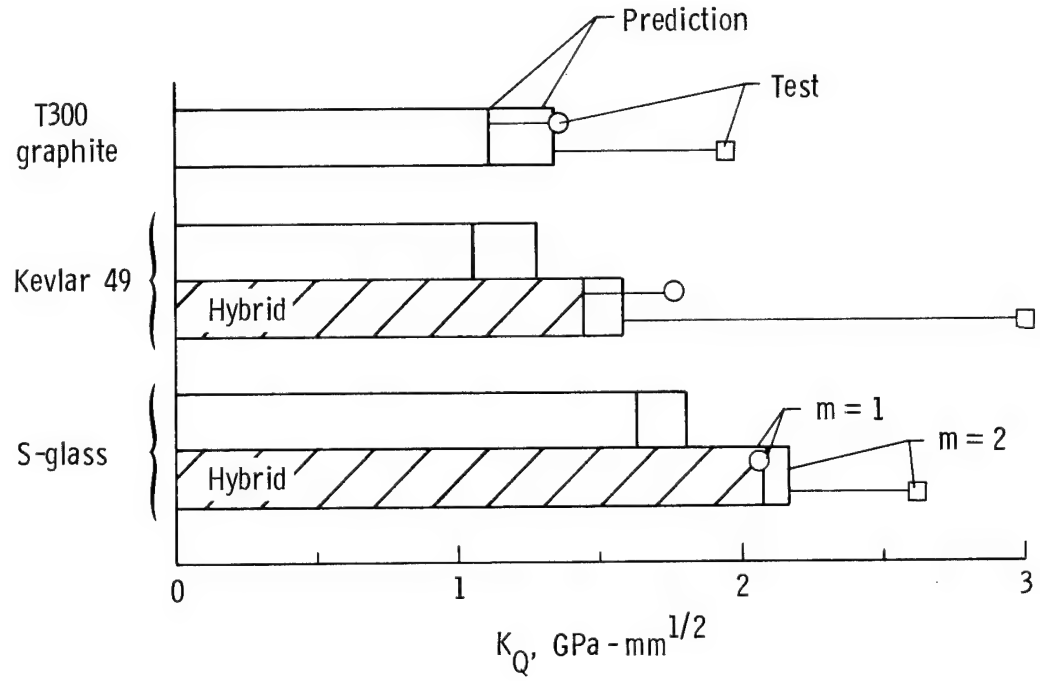

Figure 13.- Values of K_Q for $[45/0_m/-45/90]_{2s}$ hybrids with 5208 matrix. For hybrids, off-axis plies are T300 graphite.

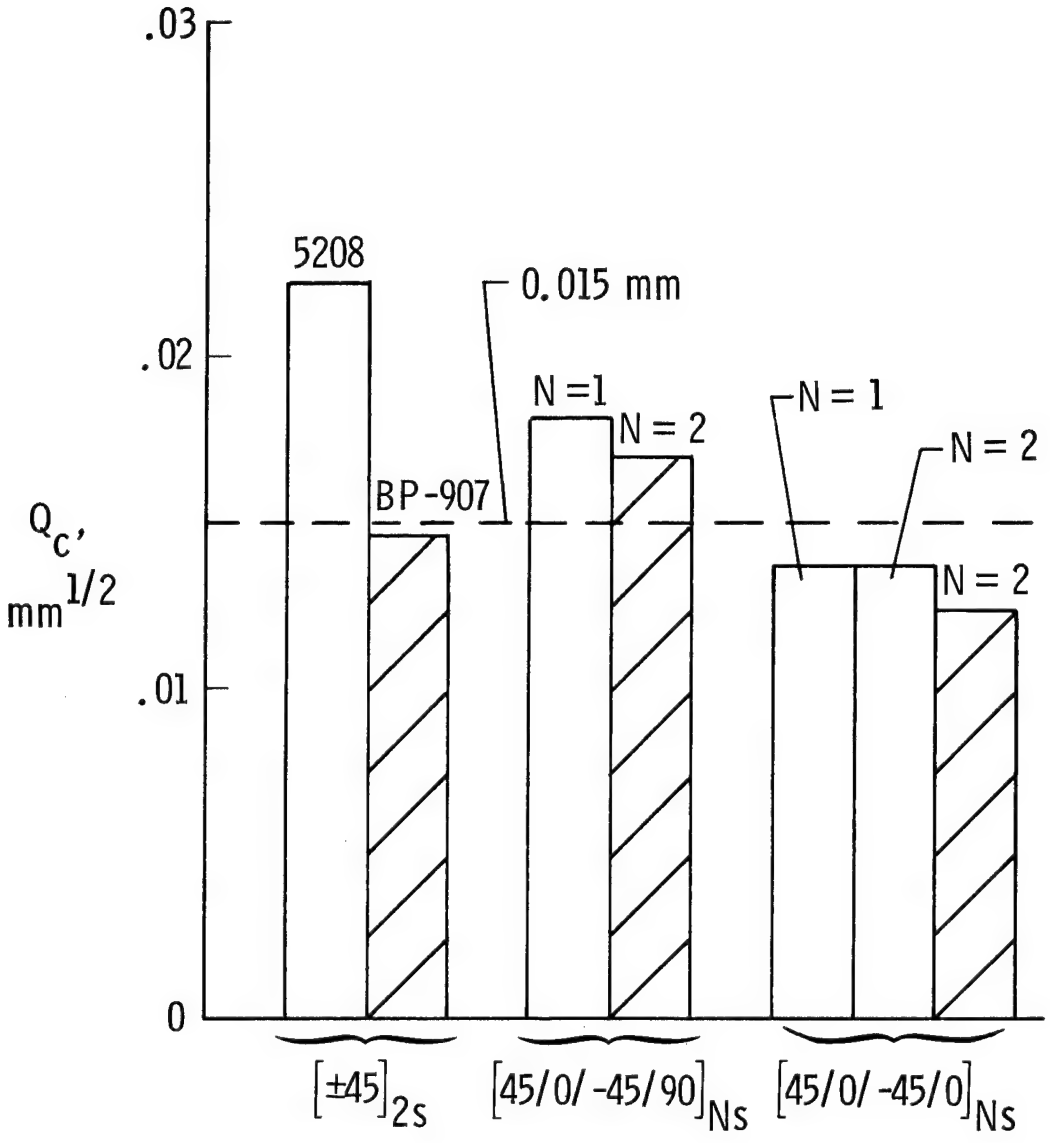

Figure 14.- Effect of matrix on Q_c.

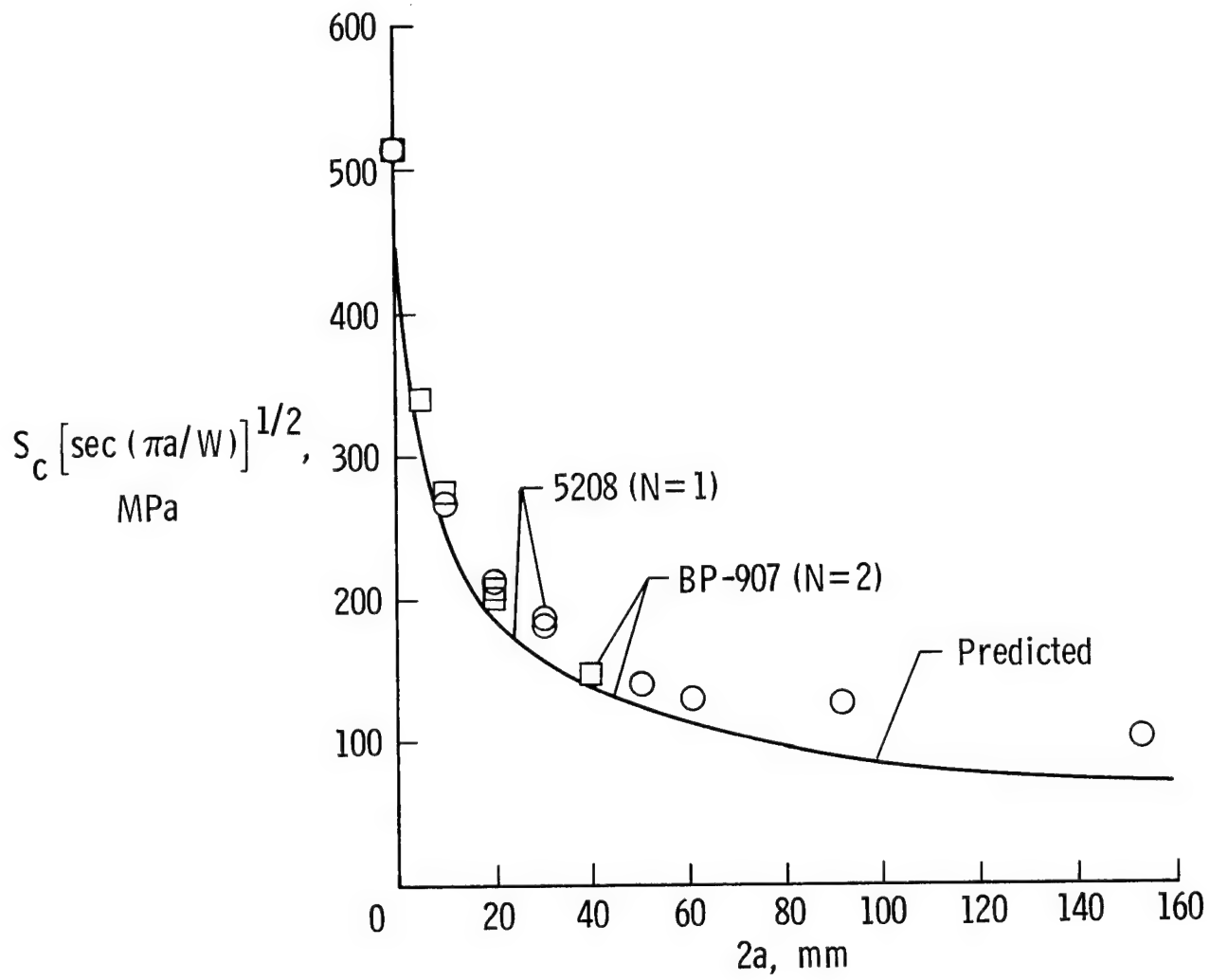

(a) $[45/0/-45/90]_{Ns}$.

Figure 15.- Effect of matrix on strength. BP-907 strengths were adjusted for differences between V_f of BP-907 and 5208.

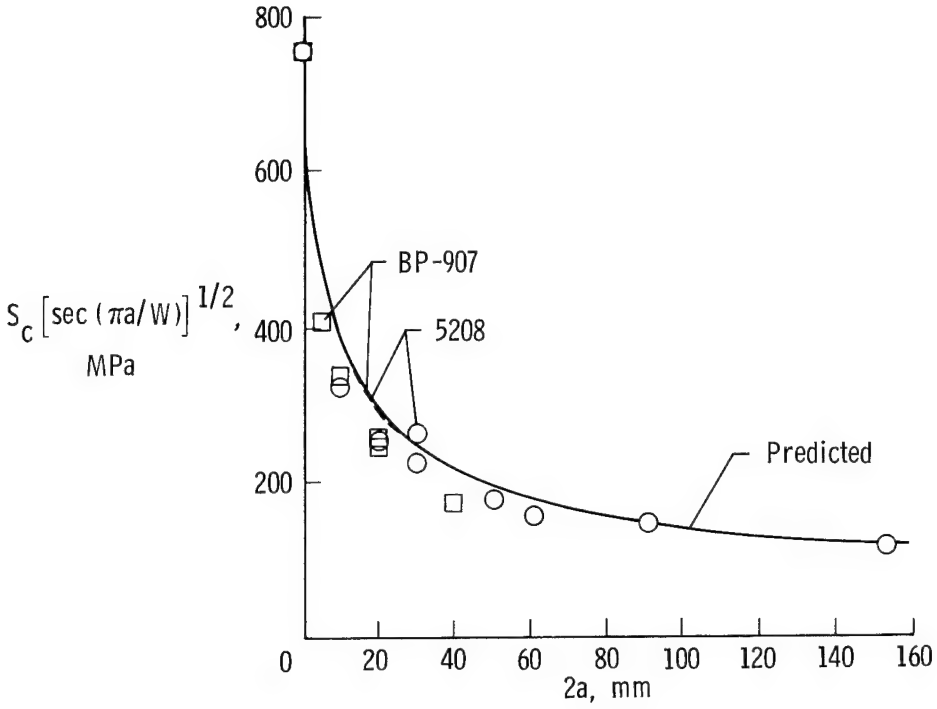

(b) $[45/0/-45/0]_{2s}$.

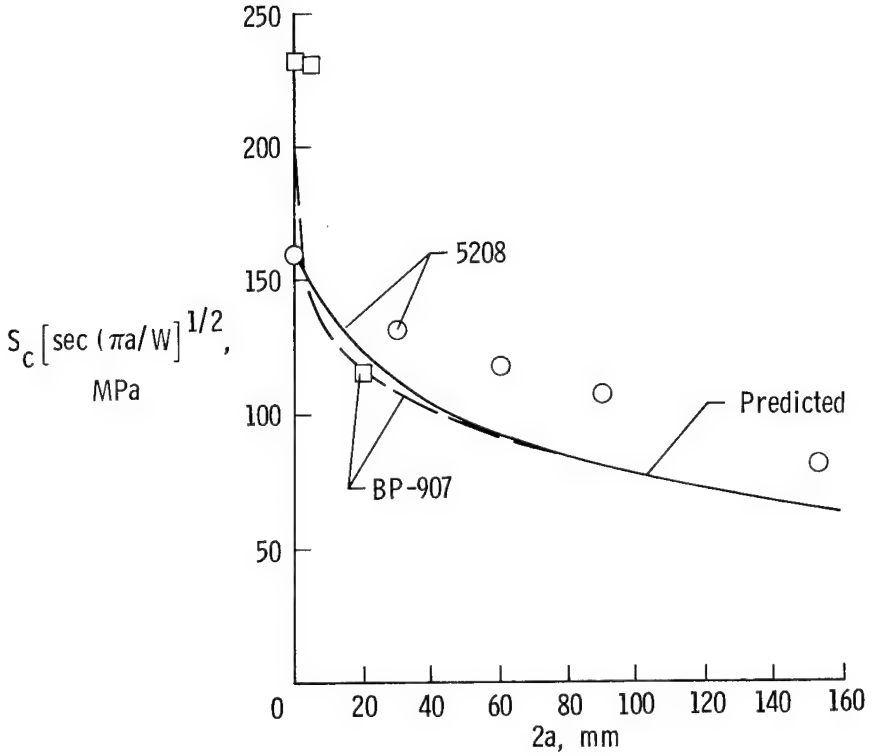

(c) $[\pm 45]_{2s}$.

Figure 15.- Concluded.

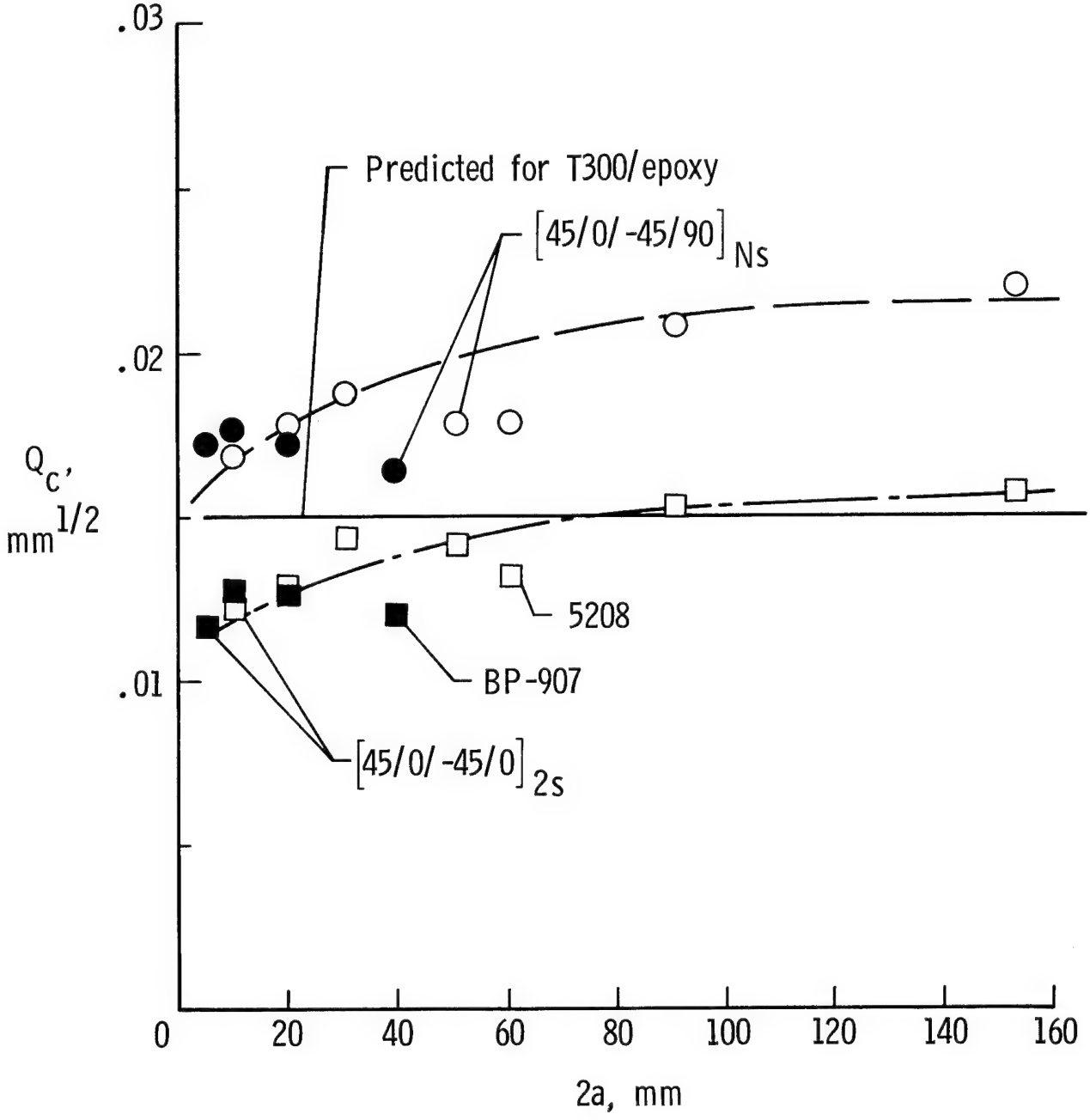

Figure 16.- Q_c plotted against 2a for $[45/0/-45/90]_{Ns}$ and $[45/0/-45/0]_{2s}$ 5208 and BP-907.

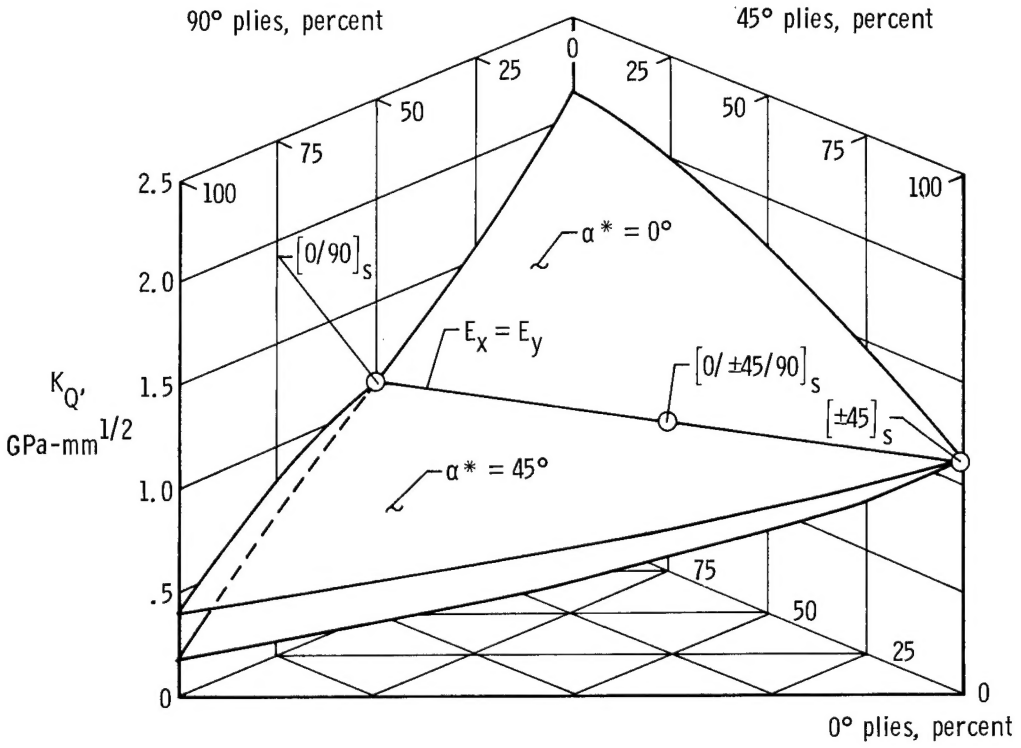

Figure 17.- Effect of lay-up on K_Q for $[0_m/\pm45_n/90]_s$ T300/5208.

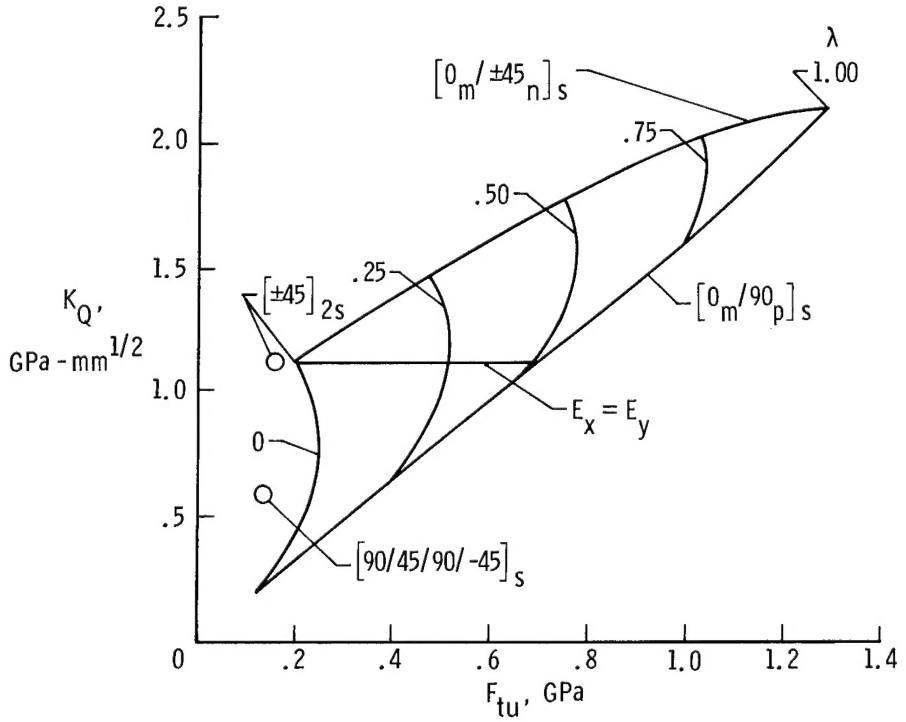

Figure 18.- K_Q plotted against F_{tu} for $[0_m/\pm45_n/90_p]_s$ T300/5208. $\alpha^* = 0°$.

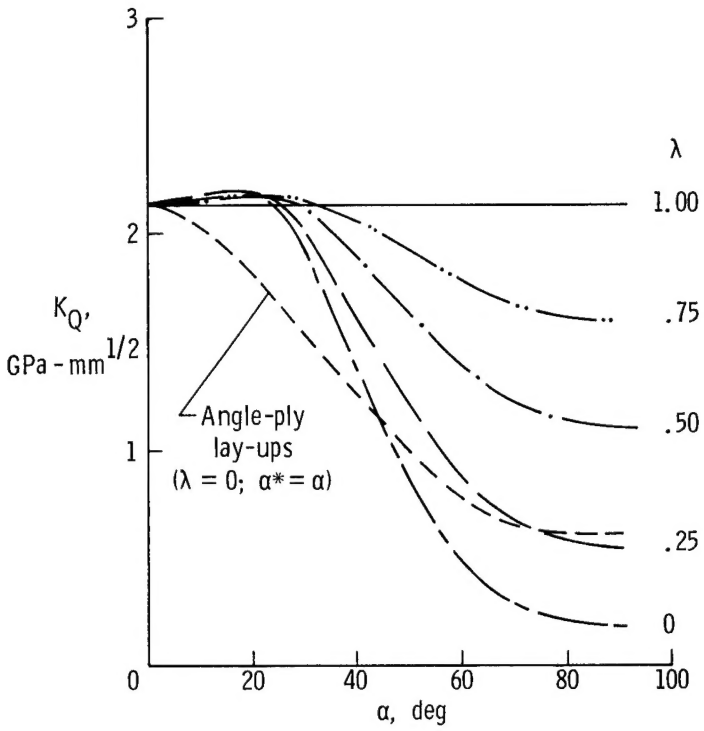

Figure 19.- Effect of lay-up on K_Q for $[0_m/\pm\alpha_n]_s$ T300/5208. $\alpha^* = 0°$.

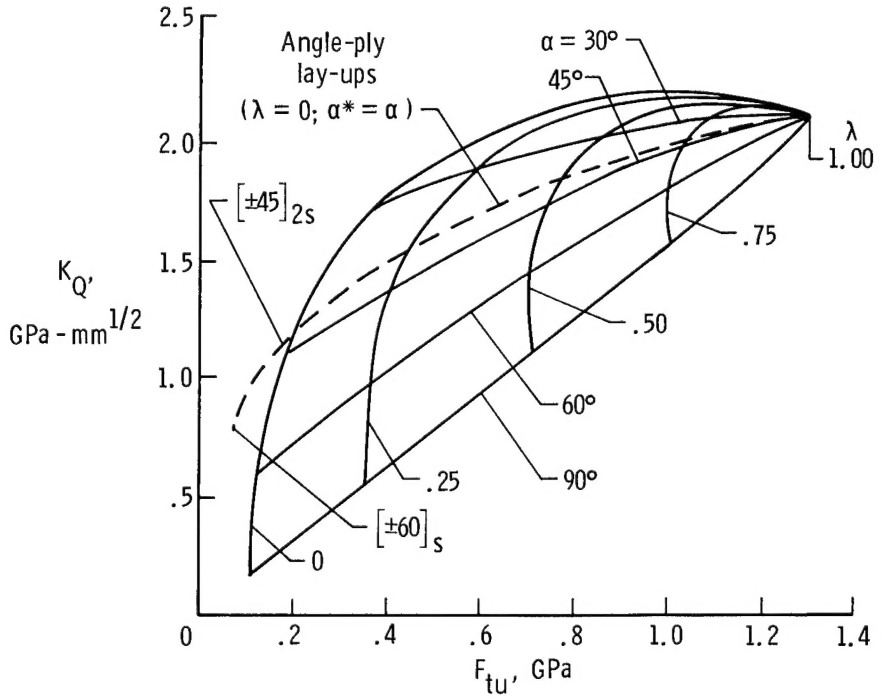

Figure 20.- K_Q plotted against F_{tu} for $[0_m/\pm\alpha_n]_s$ T300/5208. $\alpha^* = 0°$.

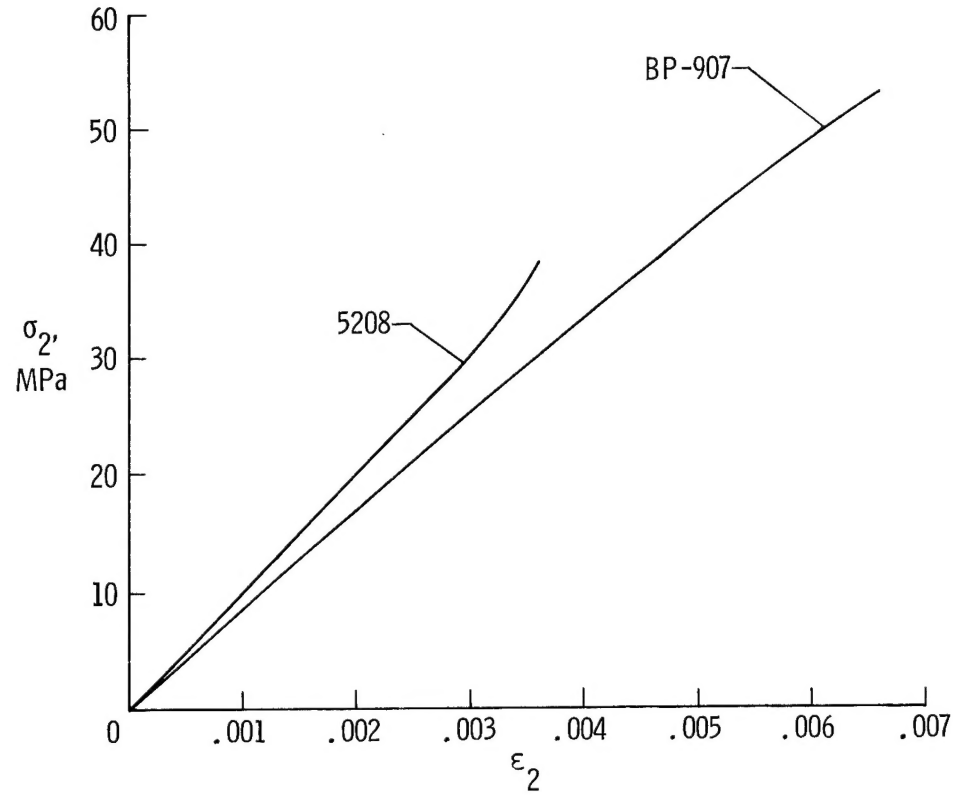

(a) $[90]_{8T}$ in tension.

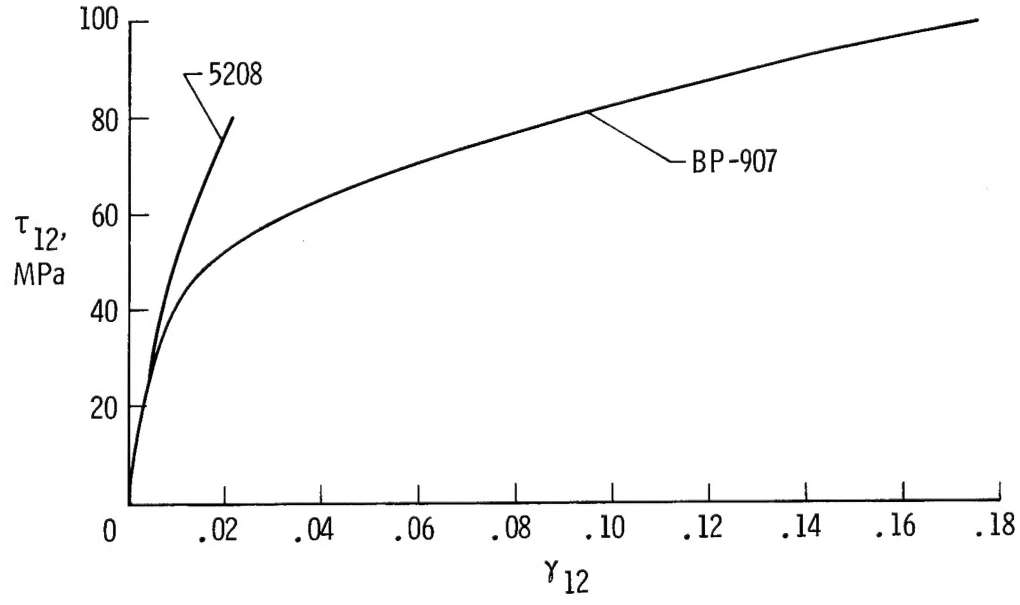

(b) $[\pm 45]_{2s}$ in tension.

Figure 21.- Stress-strain curves for 5208 and BP-907 lamina.

1. Report No.	2. Government Accession No.	3. Recipient's Catalog No.
NASA TP-2370		

4. Title and Subtitle	5. Report Date
FRACTURE TOUGHNESS OF FIBROUS COMPOSITE MATERIALS	November 1984
	6. Performing Organization Code 506-53-23-05
7. Author(s) C. C. Poe, Jr.	8. Performing Organization Report No. L-15848
	10. Work Unit No.
9. Performing Organization Name and Address NASA Langley Research Center Hampton, VA 23665	11. Contract or Grant No.
	13. Type of Report and Period Covered Technical Paper
12. Sponsoring Agency Name and Address National Aeronautics and Space Administration Washington, DC 20546	14. Sponsoring Agency Code

15. Supplementary Notes

16. Abstract

Laminates with various proportions of 0°, ±45°, and 90° plies were fabricated from T300/5208 and T300/BP-907 graphite/epoxy prepreg tape material. The fracture toughness of each laminate orientation or lay-up was determined by testing center-cracked specimens, and it was also predicted with the general fracture-toughness parameter. The predictions were good except when crack-tip splitting was large, at which time the toughness and strengths tended to be underpredicted. By using predictions, a parametric study was also made of factors that influence fracture toughness. Fiber and matrix properties as well as lay-up were investigated, and both $[0_m/\pm45_n/90_p]_s$ and $[0_m/\pm\alpha_n]_s$ lay-ups were considered. Without crack-tip splitting, fracture toughness increases in proportion to fiber strength and fiber volume fraction, increases linearly with E_{22}/E_{11}, is largest when the modulus of non-0° fibers is greater than that of 0° fibers, and is smallest for $[0_m/90_p]_s$ lay-ups. (The E_{11} and E_{22} are Young's moduli of the lamina parallel to and normal to the direction of the fibers, respectively.) For a given proportion of 0° plies, the most notch-sensitive lay-ups are $[0_m/90_p]_s$ and the least sensitive are $[0_m/\pm45_n]_s$ and $[\pm\alpha]_s$. Notch sensitivity increases with the proportion of 0° plies and decreases with α. Strong, tough matrix materials, which inhibit crack-tip splitting, generally lead to minimum fracture toughness.

17. Key Words (Suggested by Author(s))

Composite materials
Fracture toughness
Graphite/epoxy
Hybrids

18. Distribution Statement

Unclassified - Unlimited

Subject Category 24

19. Security Classif. (of this report)	20. Security Classif. (of this page)	21. No. of Pages	22. Price
Unclassified	Unclassified	67	A04

For sale by the National Technical Information Service, Springfield, Virginia 22161 NASA-Langley, 1984